

Sonnet: Spectral Operator Neural Network for Multivariable Time Series Forecasting

Yuxuan Shu, Vasileios Lamos

Centre for Artificial Intelligence
Department of Computer Science
University College London
{yuxuan.shu.22, v.lamos}@ucl.ac.uk

Abstract

Multivariable time series forecasting methods can integrate information from exogenous variables, leading to significant prediction accuracy gains. The transformer architecture has been widely applied in various time series forecasting models due to its ability to capture long-range sequential dependencies. However, a naïve application of transformers often struggles to effectively model complex relationships among variables over time. To mitigate against this, we propose a novel architecture, termed **Spectral Operator Neural Network (Sonnet)**. Sonnet applies learnable wavelet transformations to the input and incorporates spectral analysis using the Koopman operator. Its predictive skill relies on the **Multivariable Coherence Attention (MVCA)**, an operation that leverages spectral coherence to model variable dependencies. Our empirical analysis shows that Sonnet yields the best performance on 34 out of 47 forecasting tasks with an average mean absolute error (MAE) reduction of 2.2% against the most competitive baseline. We further show that MVCA can remedy the deficiencies of naïve attention in various deep learning models, reducing MAE by 10.7% on average in the most challenging forecasting tasks.¹

Code & data — <https://github.com/ClaudiaShu/Sonnet>

1 Introduction

Multivariable time series (MTS) forecasting methods learn from multiple input variables to predict a single target variable (Hidalgo and Goodman 2013). MTS models are deployed in many real-life applications, such as financial modelling (Niemira and Saaty 2004; Antunes et al. 2018; Taylor and Buizza 2003; Witt and Witt 1995), numerical weather prediction (Fildes and Kourentzes 2011; Young 2018; Dalton and Bekker 2022), and computational epidemiology (Dugas et al. 2013; Shaman and Karspeck 2012; da Silva et al. 2020; Morris et al. 2023). Recent machine learning models for time series forecasting tend to emphasise multivariate formulations (Nie et al. 2023; Zeng et al. 2023; Liu et al. 2023; Ansari et al. 2024; Das et al. 2024). While such models provide important insights for integrating traditional time series forecasting into deep learning techniques, e.g. capturing seasonality (Lin et al. 2024), frequency-domain methods (Zhou et al. 2022a,b), and autoregression (Zeng et al. 2023; Nie

et al. 2023), they often overlook the benefits of leveraging external information through exogenous indicators.

In fact, empirical evidence suggests that capturing dependencies from external variables can increase the risk of overfitting for complex models (Nie et al. 2023). Moreover, existing methods that capture inter-variable dependencies (Zhang and Yan 2023; Wang et al. 2024a) have, in certain forecasting tasks, been outperformed by models that do not (Lin et al. 2024; Luo and Wang 2024a). However, this can be attributed to the choice of forecasting benchmarks, which, in many occasions, hold strong seasonal patterns (Lin et al. 2024; see also Appendix E.5), that can be effectively modelled using simpler autoregressive methods (Zeng et al. 2023; Lin et al. 2024). Additionally, models that do not capture inter-variable dependencies benefit from learning using longer look-back windows without significantly increasing modelling complexity and computational cost (Han, Ye, and Zhan 2023), making them less likely to overfit. Nevertheless, these empirical outcomes are not necessarily valid for multivariable forecasting scenarios, especially for tasks where exogenous variables have strong predictive power. In such cases, explicitly modelling interactions across variables facilitates better performance (Wang et al. 2024b; Shu and Lamos 2025).

Prior work has explored various ways in capturing inter-variable dependencies for multivariate or MTS forecasting tasks. Methods applying attention (Vaswani et al. 2017) across variables (Liu et al. 2024; Ilbert et al. 2024) can capture nonlinear dependencies, but disrupt temporal information by embedding sequences along the time dimension. Crossformer (Zhang and Yan 2023) attempts to rectify this by proposing a modified transformer structure where input is split into time series patches allowing to capture dependencies across both the time and variable dimensions at the sub-sequence level. ModernTCN (Luo and Wang 2024b), on the other hand, uses a convolutional kernel over both the variable and time dimension to jointly capture the inter- and intra-variable dependencies. However, both Crossformer and ModernTCN suffer from GPU computational overhead as the number of exogenous variables or the length of the input time series increases (Shu and Lamos 2025; Zhou et al. 2024). TimeXer (Wang et al. 2024b) models dependencies between exogenous variables and the target variable separately, and then joins their learned embeddings with a cross-attention module. DeformTime (Shu and Lamos 2025) yields su-

¹Accepted for oral presentation at AAAI 2026. This is an extended version of the conference paper.

perior results by using deformable attention to incorporate information from exogenous variables at different time steps. However, it only captures inter-variable dependencies within the reception field of a convolutional kernel, which limits the exploration of a wider range of exogenous variables.

Frequency-based analysis techniques, including those using Fourier (Bochner 1953; Sorensen et al. 1987) or wavelet transform (Varanini et al. 1997; Zhang et al. 2003; Arneodo, Grasseau, and Holschneider 1988; Farge et al. 1992; Yu, Guo, and Sano 2024), has been widely used in statistical approaches for identifying periodic patterns (Priestley 2018) as well as in machine learning methods for forecasting (Lange, Brunton, and Kutz 2021; Zhou et al. 2022a,b; Piao et al. 2024). These methods compress temporal information (due to the Fourier transform) while some of them focus on capturing intra-variable dependencies (Zhou et al. 2022a,b). Wavelet transform, albeit dependent on the chosen mother wavelet (De Moortel, Munday, and Hood 2004; Ngui et al. 2013), can maintain both time and frequency information. In the frequency domain, spectral coherence (White and Boashash 1990) serves as a powerful tool for capturing the correlation between variables at different frequencies (Stein, French, and Holden 1972; Mima and Hallett 1999). To improve input projections into the frequency domain, Lange, Brunton, and Kutz (2021) used a Koopman operator (Mezić 2005; Rowley et al. 2009; Avila and Mezić 2020; Liu et al. 2023), i.e. a spectral function that enables linear modelling of nonlinear changes to better address nonlinearities. More recently, AdaWaveNet (Yu, Guo, and Sano 2024) decomposed the input series into seasonal and long-term components, and used the wavelet transform to capture periodic information. This method accounts for inter-variable dependencies only over the seasonal components.

Motivated by the aforementioned remarks, we propose **Spectral Operator Neural Network (Sonnet)**, a model that captures MTS dependencies in the spectral domain using a learnable wavelet transform. Sonnet captures both intra- and inter-variable dependencies using a novel frequency-domain **Multivariable Coherence Attention (MVCA)** layer. Furthermore, it deploys a learnable Koopman operator for linearised transitions of temporal states (Li et al. 2020). MVCA demonstrates stand-alone effectiveness when integrated into existing architectures, outperforming naïve attention and other modified attention mechanisms. Our key contributions are:

1. We propose **Sonnet**, a novel neural network architecture for MTS forecasting that captures inter-variable dependencies via adaptable time-frequency spectral operators while enforcing stability through learnable Koopman dynamics.
2. We introduce **MVCA**, an attention mechanism designed to model interactions between variables by leveraging their spectral coherence, a frequency-domain measurement of dependency. Unlike conventional self-attention, which computes pairwise similarity via dot products, MVCA captures temporal relationships through their cross-spectral density with the inclusion of frequency information from all variables, enhancing variable dependency modelling for MTS tasks.
3. We assess forecasting accuracy on carefully curated MTS data sets, including established benchmarks comple-

mented by tasks on weather forecasting, influenza prevalence, electricity consumption, and energy prices. The weather prediction and influenza prevalence tasks support a more thorough evaluation as they include a substantial amount of exogenous variables, multiple years (≥ 10) for training, and multiple test periods (≥ 3).

4. Sonnet reduces mean absolute error (MAE) by 2.2% on average compared to the most performant baseline model (stat. sig., $p < 10^{-3}$). In the more challenging tasks of influenza and weather modelling, MAE is reduced by 3.5% and 2%, respectively. Performance gains persist as the forecasting horizon increases, demonstrating the effectiveness of Sonnet in longer-term forecasting.

2 MTS Forecasting Task Definition

We focus exclusively on **multivariable time series (MTS)** forecasting, whereby multiple input variables are used to predict a single target variable. We note that although for some baseline models multiple output variables may be present (**multivariate forecasting**), our evaluation is restricted to the prediction of one specific output. All models are trained and evaluated under a rolling window setup, with a look-back window and a forecasting horizon of L and H time steps, respectively. At each time step t , the C observed exogenous variables over L past time steps, $\{t-L+1, \dots, t\}$, are captured in an input matrix $\mathbf{X}_t \in \mathbb{R}^{L \times C}$. The autoregressive signal for the target (endogenous) variable is denoted by $\mathbf{y}_{t-\delta} \in \mathbb{R}^L$; this encompasses time steps $\{t-\delta-L+1, \dots, t-\delta\}$, where $\delta \in \mathbb{N}_0$ is an optional delay applied when the target variable is observed with a temporal lag. We capture the exogenous and endogenous input variables in $\mathbf{Z}_t = [\mathbf{X}_t, \mathbf{y}_{t-\delta}] \in \mathbb{R}^{L \times (C+1)}$. The goal is to predict the target variable at time step $t+H$, where H denotes the forecasting horizon. Hence, the output of a forecasting model is denoted by $\mathbf{y}_{t+H} \in \mathbb{R}^H$ and holds forecasts for time steps $\{t+1, \dots, t+H-1, t+H\}$. For models that conduct multivariate forecasting, the output includes predictions for all covariates and hence is denoted by $\mathbf{Y}_{t+H} = [\mathbf{X}_{t+H}, \mathbf{y}_{t+H}] \in \mathbb{R}^{H \times (C+1)}$. The forecasting task is to learn $f: \mathbf{Z}_t \rightarrow \mathbf{y}_{t+H}$ or \mathbf{Y}_{t+H} . Performance is measured based on the endogenous forecast at time step $t+H$, i.e. the last (temporally) element of \mathbf{y}_{t+H} , $y_{t+H} \in \mathbb{R}$. For notational simplicity, we omit temporal subscripts and use \mathbf{Z} for \mathbf{Z}_t , \mathbf{y} for $\mathbf{y}_{t-\delta}$, and \mathbf{X} for \mathbf{X}_t .

3 Spectral Coherence with Sonnet

In this section, we provide a detailed description of our proposed model, Sonnet. It operates in the spectral domain via a learnable wavelet transform and introduces a **Multivariable Coherence Attention (MVCA)** module to capture both inter- and intra-variable dependencies. We further use a Koopman projection layer that enables stable temporal evolution via a learned linear operator.

3.1 Joint Embedding of Input Variables

Given an input matrix $\mathbf{Z} \in \mathbb{R}^{L \times (C+1)}$ that consists of the exogenous variables $\mathbf{X} \in \mathbb{R}^{L \times C}$ and endogenous variable $\mathbf{y} \in \mathbb{R}^L$, we first obtain the embeddings of \mathbf{X} and \mathbf{y} independently. These are denoted by $\mathbf{E}_x \in \mathbb{R}^{L \times \alpha d}$ and $\mathbf{E}_y \in \mathbb{R}^{L \times (1-\alpha)d}$.

They are derived using learnable weight matrices $\mathbf{W}_x \in \mathbb{R}^{C \times \alpha d}$ and $\mathbf{W}_y \in \mathbb{R}^{1 \times (1-\alpha)d}$, as in $\mathbf{E}_x = \mathbf{X}\mathbf{W}_x$, where d is the embedding dimension and $\alpha \in [0, 1]$ a hyperparameter that controls the projected dimensionality of \mathbf{X} and \mathbf{y} in the final embedding.² By concatenating along the feature dimension, we obtain the final embedding $\mathbf{E} = [\mathbf{E}_x, \mathbf{E}_y] \in \mathbb{R}^{L \times d}$.

3.2 Learnable Wavelet Transform

We then transform the time series embedding into the wavelet space that contains both time and frequency information, to capture both fine-grained details and overall trends across various temporal resolutions (Mallat 1989; Daubechies 1990). Specifically, after obtaining the input time series embedding \mathbf{E} , we first define a set of K learnable wavelet transformations (also referred to as atoms), with the k -th atom held in a matrix $\mathbf{M}_k \in \mathbb{R}^{d \times L}$ derived by

$$\mathbf{M}_k = \exp(-\mathbf{w}_\alpha \mathbf{t}^2) \times \cos(\mathbf{w}_\beta \mathbf{t} + \mathbf{w}_\gamma \mathbf{t}^2), \quad (1)$$

where $\mathbf{t} \in \mathbb{R}^L$ is a row vector capturing normalised time steps with $t_i = i/(L-1)$ for $i = 0, \dots, L-1$, and $\mathbf{w}_\alpha, \mathbf{w}_\beta$, and $\mathbf{w}_\gamma \in \mathbb{R}^d$ are learnable weight vectors that control the shape of the wavelet, each initialised randomly from a normal distribution. In particular, \mathbf{w}_α controls the width of the Gaussian envelope, and $\mathbf{w}_\beta, \mathbf{w}_\gamma$ respectively determine the linear or quadratic frequency modulation of the generated cosine waveforms. This formulation enables the atoms to adapt to localised time-frequency structures in the data. The time series embedding $\mathbf{E} \in \mathbb{R}^{L \times d}$ is then transformed into the wavelet space by projecting it onto each of the wavelet atoms $\mathbf{M}_k \in \mathbb{R}^{d \times L}$ using $\mathbf{P}_k = \mathbf{E} \odot \mathbf{M}_k^\top$, where $\mathbf{P}_k \in \mathbb{R}^{L \times d}$ denotes the embedding's projection for the k -th atom, and \odot is element-wise multiplication. The transformed wavelet across all K atoms is denoted by $\mathbf{P} \in \mathbb{R}^{K \times L \times d}$. The aforementioned steps help to preserve temporal structure while decomposing the input into multi-resolution time-frequency components using adaptive wavelet transforms that can capture both short- and long-term patterns in the data.

3.3 Multivariable Coherence Attention (MVCA)

In MTS forecasting, input variables can be both auto-correlated (to their own past values) and cross-correlated (to each other). To improve learning from these correlations, we propose MVCA, a module that supplements the standard attention. MVCA can capture inter- and intra-variable dependencies within the frequency domain using spectral density coherence. Its premise is that variables with a higher spectral coherence should contribute more to the attention output. MVCA can be used in place of any naïve attention module used in a forecasting method.

Given the obtained input embedding matrix in wavelet space $\mathbf{P} \in \mathbb{R}^{K \times L \times d}$, where L and d are the time and variable dimension, K is the number of wavelets after transformation, we first linearly project it to query, key and value embeddings,

²We make sure that both products αd and $(1-\alpha)d \in \mathbb{N}$ to avoid dimension mismatch caused by rounding. For $\alpha = 0$, the forecasting is based on the historical values of the target variable only, collapsing to an autoregressive setting. For $\alpha = 1$, forecasting depends entirely on the exogenous variables.

denoted as \mathbf{Q}, \mathbf{K} , and $\mathbf{V} \in \mathbb{R}^{K \times L \times d}$, using weight matrices $\mathbf{W}_q, \mathbf{W}_k$, and $\mathbf{W}_v \in \mathbb{R}^{d \times d}$ respectively, as in $\mathbf{Q} = \mathbf{P}\mathbf{W}_q$. We then consider the embeddings from different wavelet transformations (indexed by k) as separate attention heads. Specifically, for each attention head, we obtain the sub-tensor of \mathbf{Q}, \mathbf{K} , and \mathbf{V} , denoted as $\mathbf{Q}_h, \mathbf{K}_h$, and $\mathbf{V}_h \in \mathbb{R}^{L \times d}$, as the query, key, and value embeddings. Therefore, each head captures a distinct subspace of the original embedding, where subspaces correspond to different wavelet transformations of the input. Including a multi-head structure enables the model to learn diverse dependencies in parallel (Vaswani et al. 2017).

We then apply a Fast Fourier Transform (FFT) along the variable dimension (Dudgeon and Mersereau 1984) of each transformer head to transfer the query and key embeddings to the frequency domain, i.e. $\mathbf{Q}_f = \text{FFT}(\mathbf{Q}_h)$ and $\mathbf{K}_f = \text{FFT}(\mathbf{K}_h)$, with both \mathbf{Q}_f and $\mathbf{K}_f \in \mathbb{C}^{L \times \ell}$, where $\ell = \lfloor \frac{d}{2} \rfloor + 1$. Each frequency bin in the transformed data ($\mathbf{Q}_f, \mathbf{K}_f$) contains information from all original inputs to the FFT (Lee-Thorp et al. 2022), capturing both fine-grained (high-frequency) and global (low-frequency) patterns. The cross-spectral density $\mathbf{P}_{qk} \in \mathbb{C}^{L \times \ell}$ and power-spectral densities $\mathbf{P}_{qq}, \mathbf{P}_{kk} \in \mathbb{R}^{L \times \ell}$ are obtained as follows:

$$\mathbf{P}_{qk} = \mathbf{Q}_f \odot \mathbf{K}_f^*, \mathbf{P}_{qq} = \mathbf{Q}_f \odot \mathbf{Q}_f^*, \mathbf{P}_{kk} = \mathbf{K}_f \odot \mathbf{K}_f^*, \quad (2)$$

where * denotes the complex conjugate. We average along the second dimension to obtain $\bar{\mathbf{P}}_{qk} \in \mathbb{C}^L, \bar{\mathbf{P}}_{qq}$, and $\bar{\mathbf{P}}_{kk} \in \mathbb{R}^L$ (see also Appendix B). The normalised spectral coherence $\mathbf{C}_{qk} \in \mathbb{R}^L$ is then computed using

$$\mathbf{C}_{qk} = |\bar{\mathbf{P}}_{qk}|^2 / (\bar{\mathbf{P}}_{qq} \cdot \bar{\mathbf{P}}_{kk} + \epsilon), \quad (3)$$

where $\epsilon = 10^{-6}$ mitigates division by 0. \mathbf{C}_{qk} captures the linear dependency between sequences across frequency bands. Therefore, the coherence here assigns higher importance to the time steps where the query and key hold more similar averaged values across multiple frequencies.

Following the common design of attention layers (Vaswani et al. 2017), we scale, normalise, and regularise \mathbf{C}_{qk} , i.e. $\mathbf{A}_h = \text{Dropout}(\text{Softmax}(\mathbf{C}_{qk}/\sqrt{d}))$. The attention weights $\mathbf{A}_h \in \mathbb{R}^L$ of each head are first broadcast along the feature dimension to form $\mathbf{A} \in \mathbb{R}^{L \times d}$, which is then multiplied with the value representations \mathbf{V}_h (element-wise) to produce head-specific outputs, $\mathbf{O}_h \in \mathbb{R}^{L \times d} = \mathbf{A} \odot \mathbf{V}_h$. We concatenate these outputs across all heads to obtain $\mathbf{O}_r \in \mathbb{R}^{K \times L \times d}$. We then use a 2-layer perceptron (MLP, d -dimensional layers) with Gaussian Error Linear Unit (GELU) activation to further capture nonlinearities. This is connected to a residual layer to form the output $\mathbf{O}_m \in \mathbb{R}^{K \times L \times d} = \mathbf{O}_r + \text{MLP}(\mathbf{O}_r)$. We then multiply \mathbf{O}_m with a weight matrix $\mathbf{W}_{\text{out}} \in \mathbb{R}^{d \times d}$ to obtain the output of MVCA, $\mathbf{O} \in \mathbb{R}^{K \times L \times d} = \mathbf{O}_m \mathbf{W}_{\text{out}}$.

3.4 Koopman-Guided Spectrum Evolvement

Motivated by Koopman operator theory (Mezić 2005; Rowley et al. 2009; Avila and Mezić 2020), which offers a framework for modelling nonlinear dynamics, we introduce a layer to capture the temporal evolution of time-frequency patterns in wavelet space. We aim to learn a Koopman operator with K

dimensions in the transformed space. To obtain the operator $\mathbf{K} \in \mathbb{C}^{K \times K}$, we first initialise a learnable complex-valued matrix $\mathbf{S} \in \mathbb{C}^{K \times K}$. At each forward pass, we apply QR decomposition to \mathbf{S} , and retain only the resulting unitary matrix $\mathbf{U} \in \mathbb{C}^{K \times K}$, i.e. $\mathbf{U} \leftarrow \text{QR}(\mathbf{S})$ s.t. $\mathbf{U}^\dagger \mathbf{U} = \mathbf{I}$, where \mathbf{U}^\dagger is the conjugate transpose of \mathbf{U} . Multiplying with \mathbf{U} therefore prevents data amplification or distortion.

We then initialise a learnable vector $\mathbf{p} \in \mathbb{R}^K$, where the k -th element, p_k , controls the temporal evolution (phase transformation angle) of the k -th transformation. All elements in the vector are then mapped into complex numbers, obtaining $\mathbf{v} \in \mathbb{C}^K$, where $v_k = e^{ip_k}$. We use \mathbf{v} to form a diagonal matrix $\mathbf{D} \in \mathbb{C}^{K \times K} = \text{diag}(\mathbf{v})$. The Koopman operator, \mathbf{K} , is then given by $\mathbf{K} = \mathbf{U}\mathbf{D}\mathbf{U}^\dagger$. We use \mathbf{K} to model the temporal evolution of the MVCA embedding, \mathbf{O} , after converting it to a complex form, $\mathbf{O}_c \in \mathbb{C}^{K \times L \times d}$ (the imaginary part is set to $i0$ to perform complex-valued transformations without altering the original embedding), given by $\mathbf{O}_l = \mathbf{K} \times \mathbf{O}_c$, where $\mathbf{O}_l \in \mathbb{C}^{K \times L \times d}$ is the evolved embedding after multiplication with \mathbf{K} . A conventional Koopman framework models temporal evolution recursively at each time step (Lusch, Kutz, and Brunton 2018; Avila and Mezić 2020). We instead choose to apply Koopman transformation in the frequency domain with one forward pass, which is equivalent to learning a direct transformation from the input to the output. This global projection reduces the accumulation of sequential errors while maintaining robustness in training.

3.5 Sequence Reconstruction from Wavelets

The inverse transformation reconstructs the original sequence by aggregating weights from each wavelet atom. Given the evolved state \mathbf{O}_l , we first obtain its real part denoted as $\mathbf{O}_r \in \mathbb{R}^{K \times L \times d}$. For each wavelet atom indexed by k , let $\mathbf{O}_k \in \mathbb{R}^{L \times d}$ denote the corresponding slice of \mathbf{O}_r . We then multiply it with the wavelet atom $\mathbf{M}_k \in \mathbb{R}^{d \times L}$, i.e. $\mathbf{R}_k = \mathbf{O}_k \odot \mathbf{M}_k^\top$. $\mathbf{R}_k \in \mathbb{R}^{L \times d}$ denotes the series reconstruction from the k -th atom. This operation is conducted over all K atoms. Joining all the reconstructed series forms a $K \times L \times d$ matrix. We sum over its first dimension to obtain the reconstructed embedding, denoted as $\mathbf{R} \in \mathbb{R}^{L \times d}$.

3.6 Convolutional Decoder

Finally, a 3-layer convolutional decoder transforms the learned representation. It comprises 3 1-dimensional convolutional layers with GELU activations between every 2 layers. Each layer uses kernel sizes [5, 3, 3] and paddings [2, 1, 1] respectively, followed by an adaptive average pooling layer at the end. The dimension of each layer is $[H \times 4, H \times 2, H]$, producing the final sequence representation $\mathbf{Z}_{\text{out}} \in \mathbb{R}^{H \times H}$, in accordance with the time steps of the target forecasting horizon. The result is then linearly projected using a weight vector $\mathbf{W}_z \in \mathbb{R}^H$ to generate the final output, as in $\hat{\mathbf{y}} \in \mathbb{R}^H = \mathbf{Z}_{\text{out}} \mathbf{W}_z$, in accordance with the dimensionality of the target variable.

4 Results

We assess forecasting accuracy using an expanded collection of data sets and tasks, to overcome potential biases present in

the current literature. We first compare Sonnet against other competitive baseline models. We then investigate the role of attention mechanisms in time series forecasting models by removing or replacing naïve transformers with more advanced variants, including the proposed MVCA module. We also provide an ablation study of the key components of Sonnet and seed control in Appendix E.

4.1 Experiment Settings

We conduct experiments over 12 real-world data sets. This includes 2 established benchmarks from prior papers (Zhou et al. 2021; Zeng et al. 2023), specifically the ETTh1 and ETTh2 data sets, which contain hourly electricity transformer temperature forecasting. Oil temperature is our target variable, with the remaining indicators considered as exogenous variables, following Wang et al. (2024b). We also use 2 data sets from the Darts library (Herzen et al. 2022), predicting hourly energy prices (ENER) and electricity (low-voltage) consumption (ELEC). In addition, we form weather data sets extracted from the WeatherBench repository (Rasp et al. 2020) for 5 cities from diverse geographical locations, namely London (WEA-LD), New York (WEA-NY), Hong Kong (WEA-HK), Cape Town (WEA-CT), and Singapore (WEA-SG), to support a more inclusive analysis. For each city, we sample data from its nearest grid point and obtain 5 climate indicators. We provide spatial context by including data from its eight surrounding grid points (3×3 grid) as additional exogenous variables. Following prior work on global climate forecasting (Verma, Heinonen, and Garg 2024), we resample the data to a temporal resolution of 6 hours. The forecasting target is the 850 hPa (T850) temperature, a key indicator for climate modelling (Scherrer et al. 2004; Hamill and Whitaker 2007). Finally, we include influenza-like illness (ILI) rate forecasting tasks (as in (Shu and Lampos 2025)) in 3 locations, England (ILI-ENG), and in U.S. Health & Human Services (HHS) Regions 2 (ILI-US2) and 9 (ILI-US9). In the ILI tasks, frequency time series of web searches are included as exogenous predictors. More information about the data sets is provided in Appendix A.

For the ETT tasks, we set the forecasting horizon (H) to {96, 192, 336, 720} time steps, and use a single test set of consecutive unseen instances adopting the evaluation settings in prior work (Nie et al. 2023; Liu et al. 2024). For ENER we set $H = \{24, 48, 72, 168\}$ hours ahead and use 1 year (2018) for testing. For ELEC, we use the last 2 years (2020, '21) as 2 distinct test seasons, and set H to {12, 24, 36} hours. For the WEA tasks, we form 3 test sets (years 2016, '17, '18), and set H to {4, 12, 28, 120} time steps corresponding to {1, 3, 7, 30} days. Following the same setup as in (Shu and Lampos 2025), for the ILI forecasting task, we test models on 4 consecutive influenza seasons (2015/16 to 2018/19), each time training a new model on data from previous seasons. We set $H = \{7, 14, 21, 28\}$ days (more details in Appendix D).

We compare Sonnet to 8 competitive forecasting models that, to the best of our knowledge, form the current SOTA methods: DLinear (Zeng et al. 2023), Crossformer (Zhang and Yan 2023), iTransformer (Liu et al. 2024), PatchTST (Nie et al. 2023), TimeXer (Wang et al. 2024b), Samformer (Ilbert et al. 2024), ModernTCN (Luo and Wang 2024b), and

Task	Sonnet		DeformTime		ModernTCN		Samformer		TimeXer		PatchTST		iTransformer		Crossformer		DLinear		
	<i>H</i>	MAE	ε%	MAE	ε%	MAE	ε%	MAE	ε%										
ELEC	12	0.1040	24.95	0.1162	26.68	0.1596	36.81	0.2336	53.84	0.1287	28.45	0.1419	30.76	0.1468	31.91	0.1513	30.35	0.3307	71.51
	24	0.1203	27.70	<u>0.1359</u>	<u>30.11</u>	0.1806	39.70	0.2520	56.39	0.1586	33.20	0.1545	34.04	0.1588	35.40	0.1873	35.60	0.3369	73.23
	36	0.1389	30.21	0.1729	35.81	0.2065	43.79	0.2866	62.40	0.1785	35.33	<u>0.1659</u>	<u>33.85</u>	0.1791	38.18	0.2273	39.36	0.3908	82.38
ENER	24	0.3621	65.67	0.3717	66.92	0.3752	66.53	<u>0.3703</u>	66.01	0.3733	69.59	0.3717	<u>65.89</u>	0.3838	68.36	0.3716	67.44	0.4307	76.49
	48	0.4120	71.07	0.4299	74.59	0.4154	71.74	0.4294	72.34	0.4404	77.61	0.4467	75.60	0.4386	75.63	0.4647	81.79	0.5138	89.79
	72	0.4036	70.52	0.4217	74.50	<u>0.4089</u>	<u>70.84</u>	0.4353	73.40	0.4246	74.70	0.4303	73.90	0.4276	74.19	0.4473	78.62	0.5124	89.26
	168	0.3980	68.63	0.4399	78.98	0.4497	74.86	0.4243	<u>72.28</u>	0.4493	76.76	0.4872	81.34	0.4352	74.11	<u>0.4168</u>	76.76	0.5070	87.87
ETTh1	96	0.2145	16.01	0.1941	14.96	0.2047	15.66	0.2047	15.73	0.2135	16.03	<u>0.2017</u>	<u>15.41</u>	0.2052	15.46	0.2126	16.52	0.2599	20.82
	192	0.2330	17.61	0.2116	16.08	0.2417	18.32	<u>0.2307</u>	17.64	0.2322	<u>16.96</u>	<u>0.2409</u>	<u>18.29</u>	0.2429	18.13	0.2820	21.63	0.3798	31.78
	336	<u>0.2392</u>	18.91	0.2158	16.27	0.2415	18.52	0.2523	18.94	0.2414	<u>17.34</u>	0.2559	19.29	0.2593	19.11	0.2947	22.65	0.6328	58.34
	720	<u>0.2768</u>	<u>19.73</u>	0.2862	21.81	0.2785	20.44	0.3026	23.21	0.2617	18.58	0.3087	23.89	0.2886	22.05	0.3350	24.84	0.7563	69.52
ETTh2	96	0.3098	33.04	0.3121	40.07	0.3199	40.68	0.3312	40.16	0.3346	41.04	0.3145	39.25	0.3420	42.41	0.3486	40.71	0.3349	41.68
	192	<u>0.3742</u>	<u>39.58</u>	0.3281	37.90	0.3887	47.08	0.3874	45.37	0.4154	47.07	0.3839	45.45	0.4233	47.44	0.4035	43.16	0.4084	50.67
	336	<u>0.3689</u>	<u>39.48</u>	0.3450	37.00	0.3904	50.54	0.4083	46.41	0.4041	42.26	0.4018	46.77	0.4332	45.95	0.4487	49.44	0.4710	55.53
	720	0.4335	51.62	0.3640	34.99	0.5728	63.04	0.5198	58.44	0.5135	56.17	0.4960	55.27	0.4565	45.40	0.5832	61.45	0.7981	94.67
ILI-ENG	7	1.4791	21.84	<u>1.6417</u>	28.60	1.9489	28.27	2.3475	28.31	2.8084	33.66	2.3115	27.61	2.3084	26.38	1.8698	<u>25.70</u>	2.8214	43.02
	14	1.9225	25.77	<u>2.2308</u>	33.98	2.7050	36.01	3.0290	36.63	3.4937	41.88	3.2547	37.76	3.2301	36.67	2.6543	<u>30.97</u>	3.7922	55.29
	21	2.5101	<u>36.53</u>	<u>2.6500</u>	32.70	3.0400	40.02	4.4980	54.41	4.3337	51.57	4.3192	51.11	4.2347	48.93	3.0014	40.57	4.4739	61.25
	28	<u>2.7481</u>	36.95	2.7228	40.44	3.3611	47.87	5.1598	60.78	4.9013	61.60	4.9964	59.60	4.8125	55.35	3.1983	46.15	5.0347	67.75
ILI-US2	7	0.3806	14.89	<u>0.4122</u>	<u>16.01</u>	0.4398	16.55	0.6495	24.21	0.6083	23.38	0.7097	24.51	0.6507	23.24	0.4400	16.46	0.7355	27.94
	14	0.4491	<u>18.38</u>	<u>0.4752</u>	17.73	0.5279	20.22	0.7696	30.16	0.7725	29.07	0.8635	30.11	0.7896	28.17	0.5852	20.98	0.8435	32.22
	21	0.5326	20.64	<u>0.5425</u>	<u>22.12</u>	0.5781	23.85	0.8374	31.42	0.8243	31.46	1.0286	36.70	0.8042	30.03	0.6245	22.29	0.9124	34.93
	28	0.5788	21.15	0.5538	<u>22.25</u>	<u>0.5710</u>	23.66	0.9389	36.80	0.9074	34.72	1.1525	42.61	0.9619	36.75	0.6512	23.47	0.9999	38.46
ILI-US9	7	0.2668	<u>12.98</u>	0.2622	12.26	0.2899	14.17	0.4025	19.39	0.3813	18.21	0.4116	19.34	0.4057	18.57	0.3149	14.44	0.4675	23.47
	14	0.2806	13.10	<u>0.3084</u>	<u>13.80</u>	0.3417	15.29	0.5257	24.50	0.4665	22.14	0.5020	24.09	0.4702	22.44	0.3571	17.23	0.5467	27.35
	21	0.3179	14.11	0.3179	<u>14.23</u>	0.3710	15.43	0.5415	24.22	0.5715	27.43	0.5935	29.40	0.5106	24.11	0.3418	15.90	0.6001	29.66
	28	<u>0.3675</u>	16.53	0.3532	15.75	0.3940	17.19	0.6050	27.95	0.6555	31.32	0.6665	33.35	0.6498	31.05	0.3747	<u>16.44</u>	0.6564	32.16
WEA-CT	4	1.6240	<u>9.63</u>	1.7600	10.41	1.8752	11.05	2.2265	13.09	2.2376	13.14	3.5004	20.17	2.1906	12.83	<u>1.6382</u>	9.62	3.1483	18.22
	12	3.5432	20.38	<u>3.5681</u>	<u>20.46</u>	3.7761	21.67	4.0444	23.14	3.7241	21.31	4.1910	23.99	3.9741	22.83	3.5932	20.62	4.0265	22.94
	28	3.7277	21.32	<u>3.7601</u>	<u>21.49</u>	3.9399	22.36	3.9239	22.37	3.8325	21.87	3.9405	22.48	3.9584	22.60	3.8061	21.72	3.9254	22.37
	120	3.7373	21.35	3.8040	21.67	4.0889	23.54	3.9018	22.30	3.8412	21.88	4.0547	23.02	3.9473	22.49	<u>3.7659</u>	<u>21.49</u>	4.0570	23.05
WEA-HK	4	0.6389	4.05	0.6804	4.32	0.7004	4.42	0.8097	5.10	0.8648	5.52	1.1488	7.15	0.8048	5.08	<u>0.6488</u>	<u>4.11</u>	0.9898	6.21
	12	1.2355	7.74	<u>1.2786</u>	<u>7.99</u>	1.3555	8.43	1.4006	8.70	1.3027	8.13	1.5825	9.77	1.4225	8.86	1.2896	8.08	1.5464	9.62
	28	1.4135	8.83	<u>1.4746</u>	<u>9.16</u>	1.5866	9.82	1.6226	10.05	1.5115	9.39	1.6441	10.16	1.6356	10.08	1.5282	9.45	1.6232	10.06
	120	<u>1.5469</u>	<u>9.58</u>	1.5399	9.45	1.6326	10.22	1.8843	12.06	1.7092	10.55	2.0084	12.84	1.6745	10.45	1.5931	9.73	1.8329	11.49
WEA-LD	4	1.7231	15.16	1.8753	16.31	1.9456	16.88	2.1537	18.53	2.2628	19.25	2.7602	22.93	2.1509	18.55	<u>1.7447</u>	<u>15.26</u>	2.5065	20.94
	12	2.9589	23.88	3.0214	24.15	3.2056	25.58	3.3070	26.61	3.1625	25.25	3.5406	28.33	3.3622	27.36	3.0492	24.35	3.3927	26.70
	28	3.2161	25.49	<u>3.2724</u>	<u>25.84</u>	3.5067	27.48	3.5841	27.97	3.4672	27.23	3.7365	29.42	3.6884	29.14	3.3048	25.88	3.6073	28.16
	120	3.2464	25.82	<u>3.2973</u>	<u>26.17</u>	3.8434	29.92	3.8420	30.32	3.6557	28.52	4.2344	32.40	3.8518	30.36	3.3935	26.75	3.9640	30.35
WEA-NY	4	1.2716	11.94	1.4028	13.03	1.4154	12.95	1.6003	14.44	1.7290	15.57	2.1644	19.24	1.6066	14.40	<u>1.2935</u>	<u>12.24</u>	1.9782	17.88
	12	2.4476	21.23	2.4453	21.04	2.6221	22.93	2.7069	23.57	2.6537	22.85	2.8592	24.81	2.6609	23.09	2.4494	<u>21.11</u>	2.9507	25.29
	28	2.6744	23.10	<u>2.7450</u>	<u>23.20</u>	2.9336	25.37	3.0347	26.18	2.8775	24.48	3.0956	27.01	3.0204	25.30	2.7830	23.66	3.2099	27.07
	120	2.7135	23.15	<u>2.8224</u>	<u>23.86</u>	3.3000	28.05	3.5289	33.01	3.1501	26.55	3.4086	28.78	3.1029	27.74	2.9615	24.69	3.6129	29.75
WEA-SG	4	0.3444	1.25	0.3557	1.30	0.3624	1.32	0.3925	1.43	0.3801	1.38	0.4238	1.54	0.3868	1.41	<u>0.3532</u>	<u>1.29</u>	0.4048	1.47
	12	0.4160	1.51	0.4256	1.55	0.4493	1.64	0.4784	1.74	0.4447	1.62	0.4992	1.82	0.4662	1.70	<u>0.4359</u>	<u>1.59</u>	0.4764	1.73
	28	0.4653	1.69	<u>0.4875</u>	<u>1.77</u>	0.5196	1.89	0.5421	1.97	0.4974	1.81	0.5542	2.02	0.5307	1.93	0.5003	1.82	0.5284	1.92
	120	0.4830	1.76	<u>0.5050</u>	<u>1.83</u>	0.5321	1.94	0.5221	1.90	0.5215	1.90	0.5357	1.95	0.5233	1.90	0.5212	1.89	0.5328	1.94

Table 1: Forecasting accuracy results across all tasks, methods, and forecasting horizons (H). For the ELEC/ILI/WEA tasks, we report the average performance across 2, 4, and 3 test sets, respectively (detailed breakdowns in Appendix E.1). $\epsilon\%$ denotes sMAPE. Best results are **bolded**, second best underlined. Grey background denotes the model does not outperform persistence.

DeformTime (Shu and Lamos 2025), with TimeXer and DeformTime being designed for multivariable forecasting. We also include a naïve baseline which can either be a seasonal or a standard persistence model, depending on the presence of strong seasonality. For all tasks (except ETT), we conduct hyperparameter tuning for all models. For the ETT tasks, we adopt settings from the official repositories of methods

(except for Crossformer, which did not provide this). Appendix C has further details about the baseline models.

4.2 Forecasting Accuracy of Sonnet

Prediction accuracy for all tasks is enumerated in Table 1, using Mean Absolute Error (MAE) and symmetric Mean Absolute Percentage Error (sMAPE or $\epsilon\%$) as the main evaluation

	Attention	$H = 7$ days			$H = 14$ days			$H = 21$ days			$H = 28$ days		
		ENG	US2	US9									
iTransformer	—	2.3084	0.6507	0.4057	3.2301	0.7896	0.4702	4.2347	0.8042	0.5106	4.8125	0.9619	0.6498
	¬ Attn	2.3011	0.7242	0.4475	3.2557	0.8696	0.5344	4.4729	1.0105	0.6207	5.1864	1.1667	0.7179
	FNet	2.5534	0.7665	0.4741	3.5337	0.8746	0.5550	4.6970	1.0006	0.6066	5.3153	1.1118	0.7139
	FED	3.6150	0.9286	0.5613	4.3098	1.0750	0.6527	5.8596	1.4140	0.8669	6.4196	1.5167	0.9397
	VDAB	2.4287	0.6772	0.4126	3.3093	0.8274	0.4982	3.9406	0.8485	<u>0.4992</u>	4.4975	<u>0.9068</u>	<u>0.5790</u>
	MVCA	2.2707	0.5483	0.3581	3.1233	0.7267	0.4454	<u>4.1780</u>	0.7578	0.4880	4.8705	0.8885	0.5409
SamFormer	—	2.3475	0.6495	0.4025	3.0290	0.7696	0.5257	4.4980	0.8374	0.5415	5.1598	0.9389	0.6050
	¬ Attn	2.5010	0.8245	0.5131	3.3015	0.9679	0.6047	4.1830	1.1396	0.7389	5.0136	1.2391	0.8347
	FNet	2.4812	0.7765	0.4699	3.2054	0.9202	0.5865	4.3909	0.9266	0.6443	5.0592	1.0983	0.7149
	FED	3.5217	0.9140	0.5599	4.2109	1.0519	0.6508	5.7800	1.3439	0.8519	5.9809	1.4348	0.9190
	VDAB	2.0406	<u>0.5755</u>	<u>0.3651</u>	2.9525	<u>0.7281</u>	<u>0.4505</u>	<u>4.1080</u>	<u>0.7883</u>	0.4861	4.9015	<u>0.8617</u>	<u>0.5605</u>
	MVCA	<u>2.1365</u>	0.5514	0.3609	3.2046	0.6935	0.4379	3.8033	0.7294	<u>0.4975</u>	4.7438	0.8159	0.5345
PatchTST	—	2.3115	0.7097	0.4116	3.2547	0.8635	0.5020	4.3192	1.0286	0.5935	4.9964	1.1525	0.6665
	¬ Attn	2.4723	0.7702	0.4585	3.6415	0.9017	0.5551	4.2998	1.0657	0.6472	4.8538	1.1704	0.7313
	FNet	2.8097	0.8033	0.4591	4.0342	0.9322	0.5327	4.7975	1.0341	0.5430	4.9718	1.1087	0.6279
	FED	3.6158	0.9292	0.5614	4.6572	1.0765	0.6542	5.8725	1.4043	0.8671	6.3728	1.4953	0.9306
	VDAB	2.0799	<u>0.5925</u>	<u>0.3820</u>	3.0211	<u>0.7722</u>	<u>0.4413</u>	3.8164	0.8009	0.5159	4.6044	0.8518	0.5801
	MVCA	2.0054	0.5824	0.3705	<u>3.0411</u>	0.7406	0.4291	<u>3.8627</u>	0.7871	0.4746	4.5712	0.8765	0.5491

Table 2: Performance (average MAE across 4 test seasons) of iTransformer, Samformer, and PatchTST on the ILI forecasting tasks (ILI-ENG/US2/US9) with different modifications to the naïve attention mechanism. ‘¬ Attn’ denotes the removal of the residual attention module, and FNet / FED / VDAB refer to using the attention modules proposed in FNet (2025), FEDformer (2022a), and DeformTime (2025), respectively. Best results are **bolded**, second best underlined.

metrics. For WEA tasks, sMAPE is modified to avoid small values due to Kelvin temperature units (see Appendix D.6). For ETT and ENER tasks, results are based on a single forecasting season (i.e., one train / test split per forecasting horizon), while we average over multiple seasons for other tasks.

Sonnet exhibits the overall best performance across the explored MTS forecasting tasks. Comparing Sonnet’s performance to the best-performing baseline model for each task and forecasting horizon yields an MAE reduction of 1.1% on average. Ranking-wise, Sonnet is the best-performing model on 34, and the second-best on 9 out of 47 forecasting tasks. Sonnet shows relatively inferior performance on the ETT tasks. However, the ETT data sets have only 6 exogenous variables and cover a limited training time span (2 years). Consequently, they offer a limited spectrum to gain from exploring variable dependencies, as well as insufficient historical context, both of which are elements that Sonnet leverages from. Aside from the ETT tasks, Sonnet reduces MAE by 3.3% on average. Therefore, Sonnet is more effective with more covariates and longer time spans for training. Compared to a specific forecasting model, Sonnet consistently improves accuracy, reducing MAE from 2.2% for the best-performing baseline (DeformTime) to 31.1% for the worst-performing one (DLinear). We note that the MAE performance gain over DeformTime is statistically significant based on a paired t-test across all the 47 forecasting tasks ($p = 5e - 4$). This further highlights the model’s forecasting capacity amongst a wide range of applications.

Focusing on the more challenging forecasting tasks (ILI and WEA), Sonnet outperforms baselines 25 or 26 (out of 32 tasks in total) based on sMAPE or MAE, respectively. The MAE reduction is 3.5% on average for ILI tasks and 2% for WEA tasks. Within these tasks, we also observe consistent comparative performance patterns in the baseline models. Models that do not capture inter-variable dependencies

(DLinear and PatchTST) generally offer lower predictability (Sonnet reduces their MAE by 28.8% and 29.8%), and in most ILI tasks, they cannot surpass the performance of a persistence model. In contrast, baseline models that capture inter-variable dependencies tend to perform better. Among these, those that embed the covariates along the temporal dimension, namely Samformer, TimeXer, and iTransformer, exhibit inferior performance (Sonnet reduces their MAE by 23.9%, 22.1%, and 22.9%), whereas models that preserve temporal order, namely DeformTime, ModernTCN, and Crossformer, achieve stronger results (Sonnet reduces their MAE by 3.4%, 11.1%, and 8%). Hence, in tasks with more informative covariates, preserving temporal structure while modelling inter-variable dependencies is a desirable property. We provide ablation study results in Appendix E.3 that quantify the contribution of different modules to the overall forecasting accuracy of Sonnet. Additional performance evaluation results over the entire output sequence are provided in Appendix E.8.

4.3 Effectiveness of Different Attention Modules in MTS Forecasting

We evaluate the effectiveness of the proposed attention-driven module, MVCA, by integrating it into existing forecasting models (we refer to them as base models) that originally deploy naïve transformer attention. Experiments are conducted on the ILI tasks as these are the most representative of the MTS class we are exploring: they not only contain many exogenous predictors, but also frame hard practical epidemiological modelling problems when $H = 21$ or 28 days ahead. We use Samformer (Ilbert et al. 2024), iTransformer (Liu et al. 2024), and PatchTST (Nie et al. 2023) as base models. For each one of them, we evaluate 5 attention configurations: removing the attention module altogether (¬ Attn), attention with Fourier transformer proposed by FNet (Lee-Thorp

	H	Sonnet		VDAB		FED		FNet		Naïve	
		MAE	ε%	MAE	ε%	MAE	ε%	MAE	ε%	MAE	ε%
ILI-ENG	7	1.479	21.8	1.433	20.3	5.991	77.7	1.591	27.7	1.717	25.3
	14	1.923	25.8	1.973	29.4	6.031	78.1	2.084	32.8	2.068	31.4
	21	2.510	<u>36.5</u>	<u>2.774</u>	35.2	6.045	78.2	<u>2.765</u>	39.3	2.781	37.2
	28	2.748	37.0	<u>3.060</u>	<u>44.3</u>	6.051	78.4	3.240	44.5	3.078	50.0
ILI-US2	7	0.381	14.9	0.429	16.6	1.168	45.0	0.415	18.5	0.436	17.5
	14	0.449	18.4	0.500	19.1	1.179	45.5	0.558	23.2	0.532	20.4
	21	0.533	20.6	<u>0.575</u>	20.5	1.195	46.2	0.659	25.3	0.613	23.5
	28	0.579	21.1	0.643	24.3	1.193	46.1	0.705	29.1	0.651	26.1
ILI-US9	7	0.267	13.0	0.277	13.4	0.856	41.0	0.286	14.4	0.301	13.9
	14	0.281	13.1	0.324	15.8	0.856	41.0	0.351	16.1	0.340	14.9
	21	0.318	14.1	0.319	14.5	0.857	41.0	0.379	17.8	0.404	19.2
	28	0.367	16.5	<u>0.375</u>	<u>16.8</u>	0.857	41.0	0.379	18.2	0.411	19.1
WEA-CT	4	1.624	9.6	1.714	10.1	4.359	24.6	<u>1.629</u>	<u>9.6</u>	1.726	10.2
	12	3.543	20.4	3.563	20.5	4.359	24.7	3.588	20.6	<u>3.558</u>	<u>20.5</u>
	28	3.728	21.3	3.760	21.5	4.359	24.6	3.916	22.3	<u>3.758</u>	<u>21.5</u>
	120	<u>3.737</u>	<u>21.4</u>	3.734	21.3	4.356	24.6	3.815	21.7	3.763	21.5
WEA-HK	4	0.639	4.1	0.645	4.1	2.801	17.7	<u>0.639</u>	<u>4.1</u>	0.676	4.3
	12	1.235	7.7	1.279	8.0	2.801	17.7	1.325	8.3	1.281	8.1
	28	1.413	8.8	<u>1.463</u>	<u>9.1</u>	2.808	17.8	1.494	9.3	1.475	9.2
	120	1.547	9.6	<u>1.547</u>	<u>9.6</u>	2.810	17.8	1.639	10.1	1.621	10.0
WEA-LD	4	1.723	15.2	1.814	15.8	4.668	34.9	1.740	15.3	1.811	16.0
	12	2.959	23.9	2.986	24.1	4.661	34.9	3.008	24.1	2.973	24.0
	28	3.216	25.5	3.271	25.8	4.659	34.9	3.378	26.5	<u>3.268</u>	<u>25.8</u>
	120	3.246	25.8	<u>3.319</u>	<u>26.2</u>	4.668	34.9	3.667	28.5	3.407	26.7
WEA-NY	4	1.272	11.9	1.331	12.4	5.386	40.9	1.268	11.8	1.366	12.9
	12	2.448	21.2	2.474	21.6	5.384	40.9	2.510	21.8	2.438	<u>21.5</u>
	28	2.674	23.1	<u>2.708</u>	23.4	5.387	40.9	2.797	23.8	2.724	<u>23.1</u>
	120	2.713	23.2	<u>2.788</u>	<u>23.5</u>	5.389	40.9	3.063	25.6	2.911	24.6
WEA-SG	4	0.344	1.3	0.346	1.3	0.700	2.5	0.341	1.2	0.346	1.3
	12	0.416	1.5	<u>0.421</u>	<u>1.5</u>	0.698	2.5	0.424	1.5	0.425	1.5
	28	0.465	1.7	0.473	1.7	0.698	2.5	0.495	1.8	<u>0.471</u>	<u>1.7</u>
	120	0.483	1.8	0.496	1.8	0.697	2.5	0.512	1.9	<u>0.485</u>	<u>1.8</u>

Table 3: Performance of Sonnet across the ILI and WEA tasks with different attention modules. Best results are **bolded**, second best underlined. MAE values are rounded to 3 decimals, sMAPE to 1 for spacing.

et al. 2022), the Frequency Enhanced Decomposed (FED) attention proposed in FEDformer (Zhou et al. 2022a), the variable deformable attention (VDAB) proposed by DeformTime (Shu and Lampos 2025), and ours (MVCA). Further details are provided in Appendices C.3 and D.8.

Table 2 enumerates MAEs averaged across the 4 test seasons for all forecasting horizons (sMAPEs in Appendix E.2, Table S9). Notably, for the base models, removing the attention module does not lead to significant performance degradation, with some cases even showing improved results, e.g. improved accuracy is reported for some horizons for the ILI-ENG task. This indicates that the attention modules in the base models do not always capture useful information.

By replacing naïve attention with the proposed MVCA module, we obtain significant performance gains across all ILI tasks, reducing MAE by 10.7% on average across all base models. The average MAE reduction for PatchTST is greater (15.1%) compared to the other base models (10.4% for Samformer and 6.7% for iTransformer), indicating that the application of MVCA yields enhanced performance gains

for the model that does not capture inter-variable dependencies. When compared to other modified attention modules, MVCA shows competitive performance, reducing MAE by 2.8% on average. Compared to the best-performing baseline (VDAB from DeformTime), it reduces MAE and sMAPE by 3.5% and 3%, respectively. While the gains in the ENG region are less pronounced, MVCA achieves consistently the best results across the US regions, and VDAB is the second best; both methods capture inter-variable dependencies while others do not. Comparably, replacing naïve attention with the Fourier attention modules from FEDformer and FNet results in worse performance.

4.4 Sonnet with Different Attention Variants

To understand how different attention mechanisms affect the forecasting accuracy of Sonnet, we replace the MVCA module with the aforementioned modified attention mechanisms (see section 4.3). Experiments are conducted on both the ILI and WEA forecasting tasks across all locations, forecasting horizons, and test periods. Hyperparameters are re-tuned for each attention variant using the same validation procedure. Appendix C.3 provides further details.

Results are enumerated in Table 3. Overall, using MVCA yields the best accuracy compared to other attention modules, outperforming them in 26 out of the 32 tasks (MAE). On average, it reduces the MAE and sMAPE scores by 2.9% and 2%, respectively. The most competitive baseline module is VDAB (DeformTime). MVCA outperforms it by 3.6% and 3% on average w.r.t. MAE and sMAPE, respectively. The worst-performing attention module is FED (FEDformer). MVCA reduces its MAE by 51.5%. FED focuses on capturing seasonality information using frequency transformation without considering the dependencies between variables. This shows that modelling seasonality alone is insufficient for MTS forecasting, particularly when key predictive information comes from exogenous variables. The performance obtained by using either naïve attention or FNet is similar. MVCA reduces their MAE by 7% and 6.6% on average, respectively. This is expected as FNet does not introduce learnable parameters to the naïve attention.

5 Conclusion

In this paper, we present Sonnet, a novel model for multivariable time series forecasting tasks. Sonnet operates in the spectral dimension using learnable wavelet transforms and captures variable dependencies with frequency-based coherence. It then predicts future temporal dynamics with the Koopman operator. Experiments are conducted on 12 data sets from different application domains, with 9 of them containing multiple test seasons for a more comprehensive analysis. Sonnet yields the best performance in 34 out of 47 tasks, reducing MAE by 2.2% and 1.1% on average compared to the most performant baseline overall (DeformTime) or per task (can vary), respectively. Additionally, our experiments highlight that replacing vanilla attention, present in various forecasting models, with the proposed MVCA module improves prediction accuracy by a large margin.

Acknowledgements

The authors would like to thank the RCGP for providing ILI rates for England. V. Lampos would like to acknowledge all levels of support from the EPSRC grant EP/X031276/1.

References

- Andersen, F. M.; Baldini, M.; Hansen, L. G.; and Jensen, C. L. 2017. Households' hourly electricity consumption and peak demand in Denmark. *Applied Energy*, 208: 607–619.
- Ansari, A. F.; Stella, L.; Turkmen, C.; Zhang, X.; Mercado, P.; Shen, H.; Shchur, O.; Rangapuram, S. S.; Arango, S. P.; Kapoor, S.; Zschiegner, J.; Maddix, D. C.; Mahoney, M. W.; Torkkola, K.; Wilson, A. G.; Bohlke-Schneider, M.; and Wang, Y. 2024. Chronos: Learning the Language of Time Series. *Transactions on Machine Learning Research*.
- Antunes, A.; Bonfim, D.; Monteiro, N.; and Rodrigues, P. M. 2018. Forecasting banking crises with dynamic panel probit models. *International Journal of Forecasting*, 34(2): 249–275.
- Arneodo, A.; Grasseau, G.; and Holschneider, M. 1988. Wavelet Transform of Multifractals. *Phys. Rev. Lett.*, 61: 2281–2284.
- Avila, A. M.; and Mezić, I. 2020. Data-driven analysis and forecasting of highway traffic dynamics. *Nature Communications*, 11(1): 2090.
- Bochner, S. 1953. Fourier Transforms of Time Series. *Proceedings of the National Academy of Sciences*, 39(4): 302–307.
- da Silva, R. G.; Ribeiro, M. H. D. M.; Mariani, V. C.; and Coelho, L. D. S. 2020. Forecasting Brazilian and American COVID-19 cases based on artificial intelligence coupled with climatic exogenous variables. *Chaos, Solitons & Fractals*, 139: 110027.
- Dalton, A.; and Bekker, B. 2022. Exogenous atmospheric variables as wind speed predictors in machine learning. *Applied Energy*, 319: 119257.
- Das, A.; Kong, W.; Sen, R.; and Zhou, Y. 2024. A decoder-only foundation model for time-series forecasting. In *International Conference on Machine Learning*.
- Daubechies, I. 1990. The wavelet transform, time-frequency localization and signal analysis. *IEEE Transactions on Information Theory*, 36(5): 961–1005.
- De Moortel, I.; Munday, S. A.; and Hood, A. W. 2004. Wavelet Analysis: the effect of varying basic wavelet parameters. *Solar Physics*, 222(2): 203–228.
- Dudgeon, D.; and Mersereau, R. 1984. *Multidimensional Digital Signal Processing*. Prentice-Hall. ISBN 9780136049593.
- Dugas, A. F.; Jalalpour, M.; Gel, Y.; Levin, S.; Torcaso, F.; Igusa, T.; and Rothman, R. E. 2013. Influenza forecasting with Google Flu Trends. *PLoS One*, 8(2): e56176.
- Farge, M.; et al. 1992. Wavelet transforms and their applications to turbulence. *Annual review of fluid mechanics*, 24(1): 395–458.
- Fildes, R.; and Kourntzes, N. 2011. Validation and forecasting accuracy in models of climate change. *International Journal of Forecasting*, 27(4): 968–995.
- Hamill, T. M.; and Whitaker, J. S. 2007. Ensemble calibration of 500-hPa geopotential height and 850-hPa and 2-m temperatures using reforecasts. *Monthly Weather Review*, 135(9): 3273–3280.
- Han, L.; Ye, H.; and Zhan, D. 2023. The Capacity and Robustness Trade-off: Revisiting the Channel Independent Strategy for Multivariate Time Series Forecasting. arXiv:2304.05206.
- Herzen, J.; Lässig, F.; Piazzetta, S. G.; Neuer, T.; Tafti, L.; Raille, G.; Van Pottelbergh, T.; Pasička, M.; Skrodzki, A.; Huguenin, N.; Dumonal, M.; Kościsz, J.; Bader, D.; Gusset, F.; Benheddi, M.; Williamson, C.; Kosinski, M.; Petrik, M.; and Grosch, G. 2022. Darts: User-Friendly Modern Machine Learning for Time Series. *Journal of Machine Learning Research*, 23(124): 1–6.
- Hidalgo, B.; and Goodman, M. 2013. Multivariate or multivariable regression? *American journal of public health*, 103(1): 39–40.
- Hyndman, R. J.; and Koehler, A. B. 2006. Another look at measures of forecast accuracy. *International Journal of Forecasting*, 22(4): 679–688.
- Ilbert, R.; Odonnat, A.; Feofanov, V.; Virmaux, A.; Paolo, G.; Palpanas, T.; and Redko, I. 2024. SAMformer: Unlocking the Potential of Transformers in Time Series Forecasting with Sharpness-Aware Minimization and Channel-Wise Attention. In *International Conference on Machine Learning*, volume 235. PMLR.
- Kim, T.; Kim, J.; Tae, Y.; Park, C.; Choi, J.-H.; and Choo, J. 2022. Reversible Instance Normalization for Accurate Time-Series Forecasting against Distribution Shift. In *International Conference on Learning Representations*.
- Lange, H.; Brunton, S. L.; and Kutz, J. N. 2021. From Fourier to Koopman: Spectral Methods for Long-term Time Series Prediction. *Journal of Machine Learning Research*, 22(41): 1–38.
- Lee-Thorp, J.; Ainslie, J.; Eckstein, I.; and Ontanon, S. 2022. FNet: Mixing Tokens with Fourier Transforms. In *Proceedings of the 2022 Conference of the North American Chapter of the Association for Computational Linguistics: Human Language Technologies*, 4296–4313.
- Li, Y.; He, H.; Wu, J.; Katabi, D.; and Torralba, A. 2020. Learning Compositional Koopman Operators for Model-Based Control. In *International Conference on Learning Representations*.
- Lin, S.; Lin, W.; HU, X.; Wu, W.; Mo, R.; and Zhong, H. 2024. CycleNet: Enhancing Time Series Forecasting through Modeling Periodic Patterns. In *The Annual Conference on Neural Information Processing Systems*.
- Liu, Y.; Hu, T.; Zhang, H.; Wu, H.; Wang, S.; Ma, L.; and Long, M. 2024. iTransformer: Inverted Transformers Are Effective for Time Series Forecasting. In *International Conference on Learning Representations*.
- Liu, Y.; Li, C.; Wang, J.; and Long, M. 2023. Koopa: Learning Non-stationary Time Series Dynamics with Koopman Predictors. In *Conference on Neural Information Processing Systems*.
- Luo, D.; and Wang, X. 2024a. DeformableTST: Transformer for Time Series Forecasting without Over-reliance on Patching. In *The Annual Conference on Neural Information Processing Systems*.
- Luo, D.; and Wang, X. 2024b. ModernTCN: A Modern Pure Convolution Structure for General Time Series Analysis. In *International Conference on Learning Representations*.
- Lusch, B.; Kutz, J. N.; and Brunton, S. L. 2018. Deep learning for universal linear embeddings of nonlinear dynamics. *Nature Communications*, 9(1): 4950.
- Mallat, S. 1989. A theory for multiresolution signal decomposition: the wavelet representation. *IEEE Transactions on Pattern Analysis and Machine Intelligence*, 11(7): 674–693.
- Mezić, I. 2005. Spectral Properties of Dynamical Systems, Model Reduction and Decompositions. *Nonlinear Dynamics*, 41(1): 309–325.
- Mima, T.; and Hallett, M. 1999. Corticomuscular Coherence: A Review. *Journal of Clinical Neurophysiology*, 16(6).

- Morris, M.; Hayes, P.; Cox, I. J.; and Lampos, V. 2023. Neural network models for influenza forecasting with associated uncertainty using Web search activity trends. *PLoS Computational Biology*, 19(8): e1011392.
- Ngui, W. K.; Leong, M. S.; Hee, L. M.; and Abdelrhman, A. M. 2013. Wavelet analysis: mother wavelet selection methods. *Applied mechanics and materials*, 393: 953–958.
- Nguyen, T.; Brandstetter, J.; Kapoor, A.; Gupta, J. K.; and Grover, A. 2023. ClimaX: A foundation model for weather and climate. arXiv:2301.10343.
- Nie, Y.; Nguyen, N. H.; Sinthong, P.; and Kalagnanam, J. 2023. A Time Series is Worth 64 Words: Long-term Forecasting with Transformers. In *International Conference on Learning Representations*.
- Niemira, M. P.; and Saaty, T. L. 2004. An Analytic Network Process model for financial-crisis forecasting. *International Journal of Forecasting*, 20(4): 573–587.
- Piao, X.; Chen, Z.; Murayama, T.; Matsubara, Y.; and Sakurai, Y. 2024. Fredformer: Frequency Debaised Transformer for Time Series Forecasting. In *Proceedings of the 30th ACM SIGKDD Conference on Knowledge Discovery and Data Mining*, 2400–2410.
- Priestley, M. B. 2018. The Spectral Analysis of Time Series. *Journal of the Royal Statistical Society Series A: Statistics in Society*, 151(3): 573–574.
- Rasp, S.; Dueben, P. D.; Scher, S.; Weyn, J. A.; Mouatadid, S.; and Thuerey, N. 2020. WeatherBench: a benchmark data set for data-driven weather forecasting. *Journal of Advances in Modeling Earth Systems*, 12(11): e2020MS002203.
- Reich, N. G.; McGowan, C. J.; Yamana, T. K.; Tushar, A.; Ray, E. L.; Osthus, D.; Kandula, S.; Brooks, L. C.; Crawford-Crudell, W.; Gibson, G. C.; et al. 2019. Accuracy of real-time multi-model ensemble forecasts for seasonal influenza in the U.S. *PLoS Computational Biology*, 15(11): e1007486.
- Rowley, C. W.; Mezić, I.; Bagheri, S.; Schlatter, P.; and Henningson, D. S. 2009. Spectral analysis of nonlinear flows. *Journal of Fluid Mechanics*, 641: 115–127.
- Scherrer, S. C.; Appenzeller, C.; Eckert, P.; and Cattani, D. 2004. Analysis of the spread–skill relations using the ECMWF ensemble prediction system over Europe. *Weather and Forecasting*, 19(3): 552–565.
- Shaman, J.; and Karspeck, A. 2012. Forecasting seasonal outbreaks of influenza. *PNAS*, 109(50): 20425–20430.
- Shu, Y.; and Lampos, V. 2025. DEFORMTIME: Capturing Variable Dependencies with Deformable Attention for Time Series Forecasting. *Transactions on Machine Learning Research*.
- Sorensen, H.; Jones, D.; Heideman, M.; and Burrus, C. 1987. Real-valued fast Fourier transform algorithms. *IEEE Transactions on Acoustics, Speech, and Signal Processing*, 35(6): 849–863.
- Stein, R. B.; French, A. S.; and Holden, A. V. 1972. The Frequency Response, Coherence, and Information Capacity of Two Neuronal Models. *Biophysical Journal*, 12(3): 295–322.
- Taylor, J. W.; and Buizza, R. 2003. Using weather ensemble predictions in electricity demand forecasting. *International Journal of Forecasting*, 19(1): 57–70.
- Varanini, M.; De Paolis, G.; Emdin, M.; Macerata, A.; Pola, S.; Cipriani, M.; and Marchesi, C. 1997. Spectral analysis of cardiovascular time series by the S-transform. In *Computers in Cardiology 1997*, 383–386.
- Vaswani, A.; Shazeer, N.; Parmar, N.; Uszkoreit, J.; Jones, L.; Gomez, A. N.; Kaiser, Ł.; and Polosukhin, I. 2017. Attention is All you Need. In *Advances in Neural Information Processing Systems*.
- Verma, Y.; Heinonen, M.; and Garg, V. 2024. ClimODE: Climate and Weather Forecasting with Physics-informed Neural ODEs. In *The Twelfth International Conference on Learning Representations*.
- Wagner, M.; Lampos, V.; Cox, I. J.; and Pebody, R. 2018. The added value of online user-generated content in traditional methods for influenza surveillance. *Scientific Reports*, 8(13963).
- Wang, S.; Wu, H.; Shi, X.; Hu, T.; Luo, H.; Ma, L.; Zhang, J. Y.; and Zhou, J. 2024a. TimeMixer: Decomposable Multiscale Mixing for Time Series Forecasting. In *International Conference on Learning Representations*.
- Wang, Y.; Wu, H.; Dong, J.; Qin, G.; Zhang, H.; Liu, Y.; Qiu, Y.; Wang, J.; and Long, M. 2024b. TimeXer: Empowering Transformers for Time Series Forecasting with Exogenous Variables. In *The Annual Conference on Neural Information Processing Systems*.
- White, L.; and Boashash, B. 1990. Cross spectral analysis of non-stationary processes. *IEEE Transactions on Information Theory*, 36(4): 830–835.
- Witt, S. F.; and Witt, C. A. 1995. Forecasting tourism demand: A review of empirical research. *International Journal of Forecasting*, 11(3): 447–475.
- Young, P. C. 2018. Data-based mechanistic modelling and forecasting globally averaged surface temperature. *International Journal of Forecasting*, 34(2): 314–335.
- Yu, H.; Guo, P.; and Sano, A. 2024. AdaWaveNet: Adaptive Wavelet Network for Time Series Analysis. *Transactions on Machine Learning Research*.
- Yukseltan, E.; Yucekaya, A.; and Bilge, A. H. 2020. Hourly electricity demand forecasting using Fourier analysis with feedback. *Energy Strategy Reviews*, 31: 100524.
- Zeng, A.; Chen, M.; Zhang, L.; and Xu, Q. 2023. Are Transformers Effective for Time Series Forecasting? In *Proceedings of the AAAI Conference on Artificial Intelligence*, 11121–11128.
- Zhang, J.; Tsui, F.-C.; Wagner, M. M.; and Hogan, W. R. 2003. Detection of outbreaks from time series data using wavelet transform. *AMIA Annu Symp Proc*, 2003: 748–752.
- Zhang, Y.; and Yan, J. 2023. Crossformer: Transformer Utilizing Cross-Dimension Dependency for Multivariate Time Series Forecasting. In *International Conference on Learning Representations*.
- Zhou, H.; Zhang, S.; Peng, J.; Zhang, S.; Li, J.; Xiong, H.; and Zhang, W. 2021. Informer: Beyond Efficient Transformer for Long Sequence Time-Series Forecasting. In *Proceedings of the AAAI Conference on Artificial Intelligence*, 11106–11115.
- Zhou, T.; Ma, Z.; Wen, Q.; Wang, X.; Sun, L.; and Jin, R. 2022a. FEDformer: Frequency Enhanced Decomposed Transformer for Long-term Series Forecasting. In *Proceedings of the 39th International Conference on Machine Learning*, volume 162, 27268–27286.
- Zhou, T.; Ma, Z.; xue wang; Wen, Q.; Sun, L.; Yao, T.; Yin, W.; and Jin, R. 2022b. FiLM: Frequency improved Legendre Memory Model for Long-term Time Series Forecasting. In *Advances in Neural Information Processing Systems*.
- Zhou, X.; Ye, J.; Zhao, S.; Jin, M.; Yang, C.; Wen, Y.; and Yuan, X. 2024. EfficANet: Efficient Time Series Forecasting with Convolutional Attention. arXiv:2411.04669.

Supplementary Materials

A Data sets for multivariable time series forecasting

In this section, we provide a detailed description of all the data sets used in our MTS forecasting experiments. The weather data set that is formed by us is available in our code and data repository.

A.1 Hourly electricity transformer temperature prediction

The Hourly Electricity transformer temperature (ETTh1 and ETTh2) data sets are two widely used benchmarks in time series forecasting, obtained from 2 different counties in China (Zhou et al. 2021).³ The target variable of both data sets is the oil temperature. They contain 6 exogenous variables capturing power load attributes. Both data sets cover the period from July 1, 2016, to June 26, 2018. We use only a subset of 14,400 time steps starting from July 1, 2016, to match prior evaluation setups of the models that we are comparing to (Nie et al. 2023; Liu et al. 2024; Shu and Lampos 2025). Within the subset, the first 8,640 time steps are used for training, the next 2,880 for validation, and the last 2,880 for testing.

A.2 Electricity consumption prediction

The Electricity Consumption (ELEC) data set provides the electricity consumption records for Zurich (Switzerland), collected every 15 minutes.⁴ ELEC contains measurements for both residential households (recorded at low voltage) and commercial businesses (recorded at medium voltage). We choose the electricity consumption of households as our target variable for prediction. External predictors of the electricity consumption include 8 weather-related covariates recorded hourly by a weather station in the city of Zurich.

Note that for some time intervals, certain predictor values may be missing. These are imputed using linear interpolation. We then resample rates to an hourly frequency following prior work in electricity consumption prediction (Andersen et al. 2017; Yukseltan, Yucekaya, and Bilge 2020).

For the electricity consumption task, we use two test periods, years 2020 (8,784 time steps, including the leap day) and 2021 (8,760 time steps). The year preceding the test year is used as the validation (8,760 and 8,784 time steps, respectively), while the 4 years before validation form the training set (35,064 in both evaluations).

A.3 Energy price prediction

The energy price (ENER) data set contains 4 years of electrical consumption, generation, and pricing data, with the main target of predicting the actual energy price in Spain.⁵ Note

³ETTh1/h2, github.com/zhouhaoyi/ETDataset

⁴Electricity data set, github.com/unit8co/darts

⁵Energy price data set, github.com/unit8co/darts

that the original data sets have 27 exogenous variables in total. However, 8 variables consist entirely of zeros or missing values, which do not provide useful information for forecasting purposes. We therefore exclude these variables from the analysis and use the remaining 19. Data is sampled on an hourly basis. Data from December 31, 2014 to December 31, 2016 are used for training (17,545 samples). The subsequent year (January 1 to December 31, 2017; 8,760 samples) is used for validation. For testing, we use data from January 1, 2018, to 22:00, December 31, 2018 (8,759 samples); the price for the last hour is not available.

A.4 Weather forecasting on selected locations

We form the weather forecasting (WEA) data set using climate information extracted from the WeatherBench repository (Rasp et al. 2020), covering the period from 1979 to 2018.⁶ Data is sampled from a uniform spatial grid over the globe with a resolution of 5.625° in both latitude and longitude. Each grid point represents a distinct geographical location. To capture different climatic conditions, we select five spatially diverse cities from the grid: London (UK), New York (US), Hong Kong (China), Cape Town (South Africa), and Singapore. Among these, London, New York, and Hong Kong are located in the northern hemisphere, with Hong Kong being in the subtropical zone; Singapore lies near the equator, and Cape Town is in the southern hemisphere. The two cities that are closer to the equator (Hong Kong and Singapore) do not have strong seasonal temperature fluctuations over the year. Consequently, we expect models to yield lower prediction errors at these two locations. For each city, climate data is sampled from the nearest grid point to its coordinates.⁷ Specifically, we obtain the absolute distance in both latitude and longitude between each city and all grid points, and select the grid point with the smallest distance along both axes. The forecasting target is the 850 hPa temperature in Kelvin (T850) at the central grid point,⁸ which is an important climate indicator that has been widely used in climate research (Scherrer et al. 2004; Hamill and Whitaker 2007). To form exogenous inputs, we include four other climate variables at each selected grid point following prior work (Nguyen et al. 2023; Verma, Heinonen, and Garg 2024). These are the 500 hPa geopotential (Z500), 2-meter air temperature (t2m), 10-meter zonal wind (u10), and 10-meter meridional wind (v10). We also include these 4 variables and T850 from the surrounding eight grid points, forming a 3×3 spatial window centred on each selected grid, resulting in 44 exogenous variables in total. The data is resampled to maintain a temporal resolution of 6 hours similarly to Verma, Heinonen, and Garg (2024).

We consider 3 test seasons: years 2016, 2017, and 2018 (Jan. 1 to Dec. 31). Each test year contains 1,464, 1,460, and 1,460 time steps, respectively. The year immediately preceding a test year is used for validation (2015, 2016, and

⁶WeatherBench repository, dataserv.ub.tum.de/index.php/s/m1524895

⁷We obtain the longitude and latitude of each city using OpenStreetMap (wiki.openstreetmap.org).

⁸Further information about T850 is provided at charts.ecmwf.int/products/medium-z500-t850.

H	Model	2016			2017			2018			2019			Average		
		r	MAE	$\epsilon\%$												
7	DLinear	0.8710	2.6985	38.86	0.8769	1.6879	33.77	0.8231	4.2734	50.14	0.8906	2.6258	49.30	0.8654	2.8214	43.02
	iTransformer	0.8773	2.0645	27.26	0.8911	1.3734	24.06	0.8180	4.1077	31.26	0.8911	1.6881	<u>22.94</u>	0.8694	2.3084	26.38
	PatchTST	0.8832	1.9823	26.13	0.8744	1.4307	25.39	0.8475	3.7925	31.23	0.8526	2.0403	27.70	0.8644	2.3115	27.61
	TimeXer	0.8927	1.9807	26.29	0.8773	1.5327	29.94	0.6974	5.1695	43.18	0.7564	2.5507	35.22	0.8060	2.8084	33.66
	Samformer	0.8780	2.0244	27.60	0.8922	1.4025	25.10	0.7718	4.1902	35.01	0.8857	1.7729	25.55	0.8569	2.3475	28.31
	ModernTCN	0.9490	1.6043	<u>17.82</u>	0.9606	<u>1.1988</u>	<u>22.75</u>	0.9679	3.2340	40.55	0.9316	1.7584	31.98	0.9523	1.9489	28.27
	Crossformer	0.8879	2.3314	36.08	0.9591	0.8606	17.82	0.9234	2.9133	27.04	0.9436	<u>1.3737</u>	21.89	0.9285	1.8698	25.70
	DeformTime	0.9728	<u>1.3786</u>	<u>19.57</u>	<u>0.9665</u>	1.3083	29.49	0.9585	<u>2.6313</u>	41.40	0.9436	1.2485	23.96	<u>0.9603</u>	<u>1.6417</u>	28.60
	Sonnet	<u>0.9621</u>	1.0294	13.44	0.9772	1.2003	20.79	0.9590	2.0369	25.10	0.9590	1.6498	28.02	0.9643	1.4791	21.84
14	DLinear	0.7810	3.6354	52.29	0.7857	2.1872	42.47	0.6834	5.5368	60.91	0.8351	3.8092	65.47	0.7713	3.7922	55.29
	iTransformer	0.7731	2.7620	36.46	0.7776	1.9929	34.17	0.6576	5.7796	44.34	0.7850	2.3862	31.71	0.7483	3.2301	36.67
	PatchTST	0.8078	2.6267	35.59	0.7730	1.9562	33.55	0.6722	5.6075	43.64	0.7218	2.8284	38.25	0.7437	3.2547	37.76
	TimeXer	0.7891	2.6580	35.27	0.7910	1.9864	36.99	0.5503	6.2678	53.64	0.6646	3.0626	41.61	0.6988	3.4937	41.88
	Samformer	0.7205	3.0697	41.49	0.8113	1.7285	28.83	0.6888	4.9426	39.40	0.8246	2.3754	36.78	0.7613	3.0290	36.63
	ModernTCN	0.8814	2.1727	31.93	0.8864	1.4953	28.61	0.8905	4.6759	48.74	0.8441	2.4760	34.76	0.8756	2.7050	36.01
	Crossformer	0.7940	2.9124	41.75	0.8843	1.4711	23.39	0.8470	3.8295	30.88	0.9007	2.4044	27.86	0.8565	2.6543	30.97
	DeformTime	0.9259	<u>2.0556</u>	<u>25.36</u>	<u>0.9400</u>	<u>1.3180</u>	<u>33.86</u>	<u>0.9264</u>	<u>3.7631</u>	47.33	0.9154	1.7863	<u>29.36</u>	<u>0.9194</u>	<u>2.2308</u>	<u>33.98</u>
	Sonnet	<u>0.9025</u>	1.5327	22.20	0.9512	1.2453	21.28	0.9233	2.8313	28.62	0.9307	2.0808	30.99	0.9269	1.9225	25.77
21	DLinear	0.4466	4.1958	56.02	0.6441	2.8294	52.56	0.4920	6.9514	71.66	0.6608	3.9192	64.75	0.5609	4.4739	61.25
	iTransformer	0.5310	4.1390	55.62	0.5987	2.6718	43.65	0.4403	7.0816	55.17	0.6556	3.0464	41.29	0.5564	4.2347	48.93
	PatchTST	0.6126	3.6607	48.57	0.6214	2.6377	44.77	0.4427	7.3828	60.54	0.5861	3.5956	50.55	0.5657	4.3192	51.11
	TimeXer	0.5958	3.7654	49.46	0.6981	2.4045	41.17	0.4377	7.3686	62.71	0.5301	3.7962	52.91	0.5654	4.3337	51.57
	Samformer	0.4919	4.2610	57.57	0.5352	2.8996	43.99	0.5263	6.8716	60.01	0.4793	3.9598	56.07	0.5082	4.4980	54.41
	ModernTCN	0.7869	2.3283	27.42	0.8590	<u>1.6790</u>	<u>30.86</u>	<u>0.9085</u>	5.7489	61.11	0.8357	<u>2.4040</u>	<u>40.67</u>	0.8475	3.0400	40.02
	Crossformer	0.8113	2.6710	36.42	0.8014	1.8035	31.29	0.8504	4.5615	49.08	0.7331	2.9697	45.48	0.7991	3.0014	40.57
	DeformTime	0.8819	<u>2.1700</u>	<u>27.01</u>	0.8859	1.8980	32.65	0.9110	4.8984	<u>44.78</u>	0.9092	1.6335	26.36	0.8970	<u>2.6500</u>	32.70
	Sonnet	<u>0.8537</u>	1.9394	25.77	<u>0.8720</u>	1.5679	29.12	0.8260	3.9711	43.60	0.9042	2.5620	47.62	0.8640	2.5101	36.53
28	DLinear	0.3917	4.5039	60.30	0.5078	3.3928	60.94	0.3911	7.7738	77.58	0.5774	4.4683	72.19	0.4670	5.0347	67.75
	iTransformer	0.3492	4.9542	65.45	0.6761	2.2745	38.38	0.2947	8.3463	69.39	0.5286	3.6750	48.18	0.4622	4.8125	55.35
	PatchTST	0.4271	4.5240	60.22	0.4477	3.2658	53.01	0.3203	8.0693	65.91	0.4486	4.1265	59.27	0.4109	4.9964	59.60
	TimeXer	0.4978	4.2217	56.56	0.5523	2.8584	48.91	0.3413	8.1493	71.44	0.3337	4.3758	69.50	0.4313	4.9013	61.60
	Samformer	0.3995	4.7015	62.97	0.3194	3.5264	55.69	0.3127	8.1404	66.57	0.3636	4.2709	57.89	0.3488	5.1598	60.78
	ModernTCN	<u>0.8017</u>	<u>2.6486</u>	<u>36.17</u>	0.7628	2.6508	51.35	0.7544	4.8228	49.19	0.8152	3.3222	54.78	0.7835	3.3611	47.87
	Crossformer	0.7299	3.1253	41.56	0.8082	1.8197	33.57	0.7841	5.4882	55.97	0.9349	2.3599	53.48	0.8143	3.1983	46.15
	DeformTime	0.7919	2.6540	49.29	0.9229	<u>1.8100</u>	41.87	0.8493	4.8324	37.53	0.9499	1.5947	33.06	0.8785	2.7228	<u>40.44</u>
	Sonnet	0.8975	2.0133	31.59	<u>0.8841</u>	1.7490	33.24	0.7745	4.4605	<u>41.57</u>	0.7935	2.7698	41.41	0.8374	<u>2.7481</u>	36.95

Table S1: ILI rate forecasting results in England (ILI-ENG) with web search frequency time series as exogenous variables. We assess performance on 4 test seasons (2015/16 to 2018/19) using linear correlation (r), MAE, and sMAPE ($\epsilon\%$). Best results are **bolded**, second best underlined.

2017). Validation year 2015 contains 1,460 time steps. The training sets include data from January 1, 1980, up to the date preceding the corresponding validation year, resulting in 51,136, 52,596, and 54,060 time steps for the 3 test seasons.

A.5 Influenza-like-illness rate prediction

We construct an ILI forecasting data set for three regions: England (UK), and US HHS Regions 2 and 9, following the setup in prior work (Shu and Lamos 2025). Ground truth ILI rates are obtained from the Royal College of General Practitioners (RCGP) in England and the Centers for Disease Control and Prevention (CDC) for the US regions. Weekly ILI rates are linearly interpolated to a daily resolution. Specifically, we assume the ILI rates are reported corresponding to the middle day of each week, which is Wednesday for the US regions and Thursday for England (Shu and Lamos 2025). We also incorporate the ILI rate reporting delay of syndromic surveillance systems; in England there is a lag of $\delta = 7$ days and $\delta = 14$ days for the US regions (Wagner et al. 2018; Reich et al. 2019).

We use web search activity data (daily frequency time series of different search terms), obtained from the Google Health Trends API, as the exogenous indicators. We follow the setup of DeformTime (Shu and Lamos 2025) to form the set of search queries for our experiments.⁹ Note that for the US regions, search frequencies are collected at the state level, and the query data for each region is obtained using weighted averages based on the population of the states inside each region (New Jersey/New York is 0.32/0.68 for Region 2 and Arizona/California is 0.16/0.84 for Region 9).

We evaluate forecasting accuracy using 4 test seasons (2015/16, 2016/17, 2017/18, and 2018/19) in England and the US regions, each corresponding to a 12-month period that encompasses at least one seasonal flu outbreak. For England, each season begins on September 1 and ends on August 31 of the next year, while for the US regions, it is from August 1 to July 31 of the following year. For each test season, models are trained on the preceding 9 seasons. Validation sets

⁹Search queries can be obtained from github.com/ClaudiaShu/DeformTime.

H	Model	2016			2017			2018			2019			Average		
		r	MAE	$\epsilon\%$												
7	DLinear	0.7456	0.4982	29.23	0.7980	0.8210	31.85	0.7133	1.0910	30.82	0.8955	0.5318	19.84	0.7881	0.7355	27.94
	iTransformer	0.7986	0.3865	<u>21.30</u>	0.8171	0.7367	27.07	0.7784	0.9080	23.22	0.8545	0.5717	21.38	0.8122	0.6507	23.24
	PatchTST	0.7666	0.4290	23.78	0.7973	0.7546	26.97	0.6937	1.1018	26.52	0.8624	0.5533	20.79	0.7800	0.7097	24.51
	TimeXer	0.8024	0.4214	24.76	0.8480	0.6882	27.16	0.8494	0.8233	22.90	0.8859	0.5001	18.70	0.8464	0.6083	23.38
	Samformer	0.7549	0.4346	23.83	0.7935	0.7784	28.57	0.8563	0.8725	25.30	0.8834	0.5126	19.16	0.8220	0.6495	24.21
	ModernTCN	0.8745	0.3874	21.99	<u>0.9359</u>	0.5216	17.45	0.9569	<u>0.4782</u>	14.12	0.9535	0.3722	12.64	<u>0.9302</u>	0.4398	16.55
	Crossformer	0.8796	<u>0.3382</u>	21.39	0.9107	0.4975	18.32	0.9009	0.6309	15.61	0.9523	0.2936	10.52	0.9109	0.4400	16.46
	DeformTime	<u>0.8887</u>	0.3428	21.86	0.9463	0.4796	18.66	0.9008	0.5369	<u>12.88</u>	0.9622	0.2894	<u>10.64</u>	0.9245	<u>0.4122</u>	16.01
	Sonnet	0.9027	0.2854	16.40	0.9336	0.5471	18.68	0.9683	0.3708	11.52	<u>0.9537</u>	0.3192	12.97	0.9396	0.3806	14.89
14	DLinear	0.6546	0.5761	33.62	0.7335	0.9406	36.90	0.6007	1.2213	34.62	0.8261	0.6360	23.74	0.7037	0.8435	32.22
	iTransformer	0.6864	0.4894	26.35	0.7548	0.8934	33.26	0.6025	1.1639	30.28	0.8294	0.6115	22.78	0.7183	0.7896	28.17
	PatchTST	0.6628	0.5103	27.27	0.7350	0.9267	34.44	0.5993	1.3085	31.82	0.7922	0.7085	26.90	0.6973	0.8635	30.11
	TimeXer	0.7178	0.4823	27.24	0.7446	0.9211	36.47	0.7118	1.0505	28.09	0.8164	0.6362	24.47	0.7476	0.7725	29.07
	Samformer	0.7204	0.4929	28.49	0.7359	0.9580	37.34	0.8198	0.9533	29.98	0.7851	0.6741	24.81	0.7653	0.7696	30.16
	ModernTCN	<u>0.8093</u>	0.4647	25.78	0.9000	0.6482	23.18	0.9360	<u>0.6020</u>	17.05	<u>0.9572</u>	0.3968	<u>14.87</u>	0.9006	0.5279	20.22
	Crossformer	0.7872	<u>0.4357</u>	24.61	0.8640	0.6502	22.95	0.8057	0.8159	20.83	0.9241	0.4389	15.54	0.8453	0.5852	20.98
	DeformTime	0.8050	0.4404	<u>23.82</u>	0.9271	0.5029	18.53	0.9126	0.6351	<u>16.34</u>	0.9652	0.3226	12.21	<u>0.9025</u>	<u>0.4752</u>	17.73
	Sonnet	0.8654	0.3477	20.08	0.8832	0.6254	21.81	0.9731	0.4380	15.30	0.9499	0.3854	16.34	0.9179	0.4491	18.38
21	DLinear	0.6016	0.6023	35.11	0.6897	0.9671	38.06	0.4966	1.3272	38.76	0.7936	0.7530	27.80	0.6454	0.9124	34.93
	iTransformer	0.6418	0.4790	24.54	0.7515	0.8784	34.22	0.8230	1.0845	31.85	0.7321	0.7748	29.52	0.7371	0.8042	30.03
	PatchTST	0.5775	0.5592	29.41	0.6286	1.1661	43.41	0.5189	1.4395	38.13	0.6478	0.9495	35.86	0.5932	1.0286	36.70
	TimeXer	0.4856	0.5815	32.17	0.7739	0.8696	33.97	0.6529	1.1238	32.12	0.7482	0.7225	27.56	0.6651	0.8243	31.46
	Samformer	0.6042	0.5472	28.91	0.7109	0.9739	35.70	0.7263	1.1426	35.51	0.7586	0.6860	25.58	0.7000	0.8374	31.42
	ModernTCN	0.8104	0.4656	26.17	0.8746	0.6790	30.30	<u>0.9105</u>	0.7258	<u>20.75</u>	0.9487	0.4421	18.19	0.8860	0.5781	23.85
	Crossformer	<u>0.7729</u>	0.4634	26.54	0.8996	0.6688	25.62	0.7621	0.8882	23.17	0.9354	0.4777	13.82	0.8425	0.6245	22.29
	DeformTime	0.7414	0.4568	25.94	0.9028	0.6189	26.44	0.9313	0.6981	21.04	0.9408	0.3963	<u>15.09</u>	<u>0.8791</u>	<u>0.5425</u>	<u>22.12</u>
	Sonnet	0.7670	<u>0.4571</u>	<u>25.22</u>	0.9164	0.6012	23.16	0.8722	0.6961	18.91	0.9536	0.3759	15.28	0.8773	0.5326	20.64
28	DLinear	0.4836	0.6512	37.96	0.6112	1.0328	41.19	0.4125	1.4045	40.27	0.6840	0.8337	31.08	0.5479	0.9805	37.63
	iTransformer	0.5258	0.5949	32.54	0.6567	1.0632	41.38	0.5726	1.3053	38.82	0.6738	0.8842	34.26	0.6072	0.9619	36.75
	PatchTST	0.4013	0.6678	36.55	0.5274	1.2615	48.85	0.3903	1.6234	44.67	0.5579	1.0576	40.39	0.4692	1.1525	42.61
	TimeXer	0.3979	0.5856	32.82	0.7017	0.9748	39.33	0.6137	1.2462	35.29	0.7037	0.8229	31.45	0.6042	0.9074	34.72
	Samformer	0.4934	0.5858	31.55	0.6947	1.0083	39.01	0.6215	1.4670	50.33	0.7698	0.6945	26.31	0.6448	0.9389	36.80
	ModernTCN	<u>0.7635</u>	0.4702	<u>27.09</u>	0.8667	0.6742	27.31	0.9223	<u>0.6618</u>	19.83	<u>0.9604</u>	0.4776	20.41	<u>0.8782</u>	<u>0.5710</u>	23.66
	Crossformer	<u>0.7102</u>	<u>0.4697</u>	<u>27.38</u>	0.9064	0.7624	28.93	0.8432	0.8253	<u>20.69</u>	<u>0.8782</u>	0.5474	18.64	0.8345	0.6512	23.91
	DeformTime	0.8369	0.4716	27.21	0.9562	0.6017	<u>25.66</u>	0.9253	0.5954	17.62	0.9294	0.5463	<u>18.52</u>	0.9119	0.5538	<u>22.25</u>
	Sonnet	0.7578	0.4614	25.04	0.9140	0.6458	22.49	0.8747	0.7363	21.05	0.9609	0.4717	16.01	0.8768	0.5788	21.15

Table S2: ILI rate forecasting results in US Region 2 (ILI-US2) with web search frequency time series as exogenous variables. We assess performance on 4 test seasons (2015/16 to 2018/19) using linear correlation (r), MAE, and sMAPE ($\epsilon\%$). Best results are **bolded**, second best underlined.

are extracted from the last three seasons in the training data. Each validation set covers 180 days, containing three 60-day segments that capture the onset (from the last season), peak (from the penultimate season), and outset (the 3rd to last season) phases of an influenza season. The onset is defined as the first point followed by two weeks above a predefined ILI threshold; the peak is the point of the highest ILI rate; and the outset is the last point followed by two weeks above the threshold. These selected points are then considered as the 30th day in a 60-day validation period.

B Further information about MVCA

This section supplements Section 3.3 of the main paper. Here, we further clarify complex number operations.

In Equation 2, the cross-spectral and power-spectral density matrices are obtained using the frequency domain embeddings $\mathbf{Q}_f, \mathbf{K}_f \in \mathbb{C}^{L \times \ell}$. The obtained matrices $\mathbf{P}_{qq} = \mathbf{Q}_f \odot \mathbf{Q}_f^*$ and $\mathbf{P}_{kk} = \mathbf{K}_f \odot \mathbf{K}_f^*$ are both containing real numbers because multiplying a complex number (e.g. $z = a + ib$) by its conjugate ($a - ib$) results in its squared magnitude

($a^2 + b^2$), which is a real number.

In Equation 3, we obtain the coherence vector \mathbf{C}_{qk} using the averaged cross-spectral density matrix $\mathbf{P}_{qk} \in \mathbb{C}^{L \times \ell}$. The average of this imaginary matrix \mathbf{P}_{qk} is obtained by averaging the real and imaginary components separately. Taking the magnitude $|\overline{\mathbf{P}}_{qk}|$ then results in a real-valued vector, as magnitude is essentially the Euclidean norm (i.e., the square root of the sum of the squares of the real and imaginary parts) of each complex entry. As such, we obtain a real-valued coherence vector \mathbf{C}_{qk} .

C Baseline forecasting models and attention mechanisms

In this section, we first provide a brief description of the baseline models that we use in our experiments (Section C.1). To the best of our knowledge, they form the current state-of-the-art (SOTA) in MTS forecasting. These also include the base models that use naïve attention mechanisms, which we then replace with MVCA (Section 4.3). We also describe the attention modules that have been used in related literature

H	Model	2016			2017			2018			2019			Average		
		r	MAE	$\epsilon\%$												
7	DLinear	0.8071	0.4769	25.07	0.8092	0.3727	22.02	0.6759	0.5704	22.96	0.8925	0.4499	23.82	0.7962	0.4675	23.47
	iTransformer	0.8380	0.3736	17.55	0.8446	0.2721	16.22	0.6664	0.6856	26.00	0.9230	0.2915	14.52	0.8180	0.4057	18.57
	PatchTST	0.8248	0.3993	19.30	0.8318	0.2802	16.91	0.7068	0.6078	23.25	0.8796	0.3592	17.91	0.8107	0.4116	19.34
	TimeXer	0.8237	0.4071	20.04	0.8471	0.2669	15.50	0.7638	0.5235	20.92	0.9021	0.3277	16.36	0.8342	0.3813	18.21
	Samformer	0.8086	0.4116	19.72	0.8045	0.3049	18.05	0.7880	0.5042	19.90	0.8663	0.3893	19.91	0.8169	0.4025	19.39
	ModernTCN	0.9263	0.2615	13.08	0.8886	<u>0.2482</u>	14.86	<u>0.8706</u>	0.4745	20.37	0.9770	0.1754	8.37	0.9156	0.2899	14.17
	Crossformer	0.9305	<u>0.2556</u>	12.21	0.9524	0.2874	14.89	0.8213	0.4524	17.08	0.9435	0.2640	13.58	0.9119	0.3149	14.44
	DeformTime	0.9161	0.2437	<u>12.46</u>	<u>0.9356</u>	0.2364	11.69	0.8744	<u>0.3664</u>	<u>13.61</u>	0.9675	0.2023	11.29	0.9234	0.2622	12.26
	Sonnet	<u>0.9301</u>	0.2668	12.94	0.9293	0.2692	16.42	0.8481	0.3376	11.89	0.9693	0.1935	10.67	0.9192	0.2668	12.98
14	DLinear	0.7323	0.5767	29.99	0.7371	0.4384	25.44	0.6105	0.6635	27.69	0.8216	0.5085	26.27	0.7254	0.5467	27.35
	iTransformer	0.7837	0.4310	20.63	0.7629	0.3448	20.49	0.6138	0.6853	27.21	0.8495	0.4196	21.41	0.7525	0.4702	22.44
	PatchTST	0.7626	0.4810	23.33	0.7411	0.3524	21.48	0.6246	0.7164	28.11	0.8102	0.4583	23.44	0.7346	0.5020	24.09
	TimeXer	0.7423	0.4795	23.26	0.7872	0.3078	18.07	0.6443	0.6440	25.49	0.8261	0.4345	21.76	0.7500	0.4665	22.14
	Samformer	0.7297	0.4972	23.71	0.7555	0.3416	20.14	0.6032	0.7957	30.46	0.8117	0.4683	23.68	0.7250	0.5257	24.50
	ModernTCN	0.9250	0.3582	15.44	0.8543	0.3175	17.00	<u>0.8696</u>	0.4244	15.32	0.9320	0.2666	13.40	0.8952	0.3417	15.29
	Crossformer	0.8787	0.3333	16.05	0.8965	0.2980	16.74	0.8339	0.4325	16.91	0.9169	0.3647	19.21	0.8815	0.3571	17.23
	DeformTime	0.9033	<u>0.2962</u>	<u>14.39</u>	0.9374	<u>0.2893</u>	13.15	0.8490	0.3897	<u>14.62</u>	<u>0.9378</u>	<u>0.2584</u>	<u>13.05</u>	<u>0.9069</u>	<u>0.3084</u>	<u>13.80</u>
	Sonnet	0.9244	0.2807	12.91	0.9049	0.2832	14.71	0.8771	0.3490	13.24	0.9615	0.2096	11.51	0.9170	0.2806	13.10
21	DLinear	0.6687	0.6032	30.66	0.6920	0.4960	28.49	0.5830	0.7252	30.15	0.7778	0.5760	29.33	0.6804	0.6001	29.66
	iTransformer	0.8659	0.3645	17.75	0.7078	0.3702	21.73	0.4561	0.8642	33.94	0.8298	0.4433	23.01	0.7149	0.5106	24.11
	PatchTST	0.6899	0.5705	28.41	0.6399	0.4255	26.14	0.5214	0.7963	32.80	0.7137	0.5815	30.27	0.6412	0.5935	29.40
	TimeXer	0.6203	0.5899	29.37	0.6373	0.4132	24.19	0.5158	0.7825	31.10	0.7460	0.5006	25.04	0.6298	0.5715	27.43
	Samformer	0.7079	0.5086	24.07	0.8118	0.3403	18.93	0.5685	0.7794	27.50	0.7169	0.5378	26.37	0.7013	0.5415	24.22
	ModernTCN	<u>0.8695</u>	<u>0.3118</u>	12.39	0.8775	0.3695	16.88	0.7572	0.5057	18.36	0.8997	0.2968	<u>14.08</u>	0.8510	0.3710	15.43
	Crossformer	0.9565	<u>0.3267</u>	15.49	0.8669	0.3168	15.95	0.8777	0.3964	15.11	0.9135	0.3273	17.07	0.9036	0.3418	15.90
	DeformTime	0.8331	0.3543	15.62	<u>0.8966</u>	0.3039	<u>14.99</u>	0.9141	0.3536	13.06	<u>0.9249</u>	<u>0.2598</u>	13.27	0.8922	<u>0.3179</u>	<u>14.23</u>
	Sonnet	0.8573	0.2888	<u>13.12</u>	0.9619	0.3270	14.18	0.8359	0.4013	<u>14.37</u>	0.9382	0.2545	14.75	0.8983	0.3179	14.11
28	DLinear	0.6083	0.6496	32.81	0.6016	0.5329	30.18	0.5506	0.7893	32.75	0.7438	0.6539	32.89	0.6261	0.6564	32.16
	iTransformer	0.6984	0.5531	27.80	0.5779	0.4444	25.70	0.3211	0.9942	40.08	0.6797	0.6077	30.60	0.5693	0.6498	31.05
	PatchTST	0.6067	0.6457	32.75	0.5192	0.4903	30.18	0.4424	0.8809	36.70	0.6555	0.6492	33.78	0.5560	0.6665	33.35
	TimeXer	0.5345	0.6372	32.39	0.6320	0.4302	23.80	0.3998	0.9296	37.46	0.6127	0.6248	31.64	0.5448	0.6555	31.32
	Samformer	0.6543	0.5652	27.78	0.6646	0.3909	22.79	0.4984	0.8367	30.81	0.5980	0.6273	30.40	0.6038	0.6050	27.95
	ModernTCN	0.8552	0.3611	17.38	<u>0.9076</u>	0.3748	17.59	0.8068	0.5156	18.99	0.8645	<u>0.3245</u>	14.79	0.8585	0.3940	17.19
	Crossformer	0.8969	<u>0.3398</u>	16.47	<u>0.8346</u>	<u>0.3647</u>	16.99	0.8514	0.4365	15.42	0.8923	<u>0.3578</u>	16.87	0.8688	0.3747	<u>16.44</u>
	DeformTime	0.8888	0.3718	<u>15.55</u>	0.9046	0.3153	14.57	0.9037	0.4185	<u>16.18</u>	0.9260	0.3069	<u>16.68</u>	0.9058	0.3532	15.75
	Sonnet	0.8947	0.3072	15.45	0.9288	0.3723	16.09	0.8850	0.4497	16.70	0.8904	0.3406	17.90	0.8997	<u>0.3675</u>	16.53

Table S3: ILI rate forecasting results in US Region 9 (ILI-US9) with web search frequency time series as exogenous variables. We assess performance on 4 test seasons (2015/16 to 2018/19) using linear correlation (r), MAE, and sMAPE ($\epsilon\%$). Best results are **bolded**, second best underlined.

and which we compare to MVCA (Section C.3).

C.1 Baseline MTS forecasting models

DeformTime (Shu and Lampos 2025) is specifically designed for multivariable forecasting. It uses deformable attention to capture the dependencies across time and covariates, reaching competitive performance on MTS forecasting tasks. Based on our evaluation, DeformTime is the best-performing baseline.

ModernTCN (Luo and Wang 2024b) applies convolution along the temporal and variable axes. By leveraging large receptive fields, it effectively captures both intra-variable and inter-variable dependencies.

TimeXer (Wang et al. 2024b) is a transformer-based model that focuses on multivariable forecasting. It first embeds the exogenous variables along the sequence dimension, and then captures the exogenous information through a cross-attention mechanism.

Samformer (Ilbert et al. 2024) first embeds the input along the sequence dimension and then applies naïve attention

along the feature dimension. It conducts forecasts using a linear layer. We also include Samformer as one of the base models that deploy naïve attention.

iTransformer (Liu et al. 2024) embeds the input along the sequence dimension and deploys multiple attention layers along the variable dimension. We also include iTransformer as one of the base models.

PatchTST (Nie et al. 2023) segments time series data into patches of fixed size, treating them as input tokens to a transformer. It processes each variable independently, enabling efficient modelling of long-term dependencies. PatchTST is also used as one of the base models.

Crossformer (Zhang and Yan 2023) captures both inter- and intra-variable dependencies using a two-stage attention mechanism. Each stage is dedicated to one dependency type. The information is captured using time series patches.

DLinear (Zeng et al. 2023) uses a simpler neural network architecture (feedforward layers). It decomposes each input series into trend and seasonal components, which are then forecasted independently using linear layers. Each variable

H	Model	2016			2017			2018			Average		
		r	MAE	$\epsilon\%$									
4	DLinear	0.8341	2.3772	15.26	0.7730	2.5122	16.47	0.8422	2.6301	31.10	0.8164	2.5065	20.94
	iTransformer	0.8746	2.0626	13.39	0.8325	2.1816	14.51	0.8803	2.2087	27.76	0.8625	2.1509	18.55
	PatchTST	0.7975	2.6606	17.02	0.7233	2.7843	18.32	0.8077	2.8359	33.44	0.7762	2.7602	22.93
	TimeXer	0.8707	2.1636	14.07	0.8256	2.2316	14.69	0.8681	2.3932	29.00	0.8548	2.2628	19.25
	Samformer	0.8705	2.0649	13.40	0.8393	2.1271	14.15	0.8752	2.2692	28.04	0.8617	2.1537	18.53
	ModernTCN	0.8972	1.8388	11.88	0.8560	2.0076	13.33	0.9063	1.9904	25.41	0.8865	1.9456	16.88
	Crossformer	0.9186	1.6316	10.67	0.8788	1.8383	12.14	0.9225	1.7641	22.97	0.9066	1.7447	15.26
	DeformTime	0.9060	1.7647	11.64	0.8620	1.9632	12.78	0.9096	1.8982	24.50	0.8926	1.8753	16.31
	Sonnet	0.9206	1.6571	10.95	0.8887	1.7880	11.85	0.9269	1.7242	22.67	0.9121	1.7231	15.16
12	DLinear	0.6875	3.2620	20.14	0.5777	3.2740	20.77	0.6782	3.6422	39.20	0.6478	3.3927	26.70
	iTransformer	0.7073	3.1987	20.42	0.6167	3.2760	21.05	0.6916	3.6120	40.61	0.6719	3.3622	27.36
	PatchTST	0.6801	3.4350	21.80	0.5729	3.4499	22.13	0.6639	3.7370	41.06	0.6390	3.5406	28.33
	TimeXer	0.7286	3.0578	19.05	0.6602	3.0519	19.57	0.7360	3.3778	37.11	0.7082	3.1625	25.25
	Samformer	0.7117	3.1711	20.14	0.6352	3.1860	20.37	0.6969	3.5638	39.31	0.6812	3.3070	26.61
	ModernTCN	0.7266	3.0716	19.39	0.6476	3.1372	19.95	0.7140	3.4080	37.39	0.6961	3.2056	25.58
	Crossformer	0.7530	2.9360	18.52	0.6326	3.1054	19.77	0.7626	3.1061	34.75	0.7161	3.0492	24.35
	DeformTime	0.7403	2.9613	<u>18.51</u>	<u>0.6810</u>	<u>2.9529</u>	<u>18.83</u>	0.7600	3.1499	35.10	0.7271	<u>3.0214</u>	<u>24.15</u>
	Sonnet	0.7648	2.8561	17.98	0.6937	2.9154	18.69	0.7652	3.1051	34.98	0.7413	2.9589	23.88
28	DLinear	0.6197	3.5890	21.92	0.5479	3.3473	21.14	0.6560	3.8855	41.41	0.6078	3.6073	28.16
	iTransformer	0.6016	3.7784	23.47	0.5710	3.4687	22.17	0.6506	3.8182	41.77	0.6077	3.6884	29.14
	PatchTST	0.6130	3.7670	23.35	0.5358	3.6196	23.20	0.6436	3.8229	41.71	0.5974	3.7365	29.42
	TimeXer	0.6561	3.5155	21.56	0.6287	3.2048	20.43	0.6842	3.6813	39.69	0.6563	3.4672	27.23
	Samformer	0.6239	3.6455	22.48	0.5648	3.4061	21.46	0.6594	3.7008	39.99	0.6160	3.5841	27.97
	ModernTCN	0.6509	3.4012	20.79	0.5680	3.4846	22.16	0.6841	3.6345	39.48	0.6343	3.5067	27.48
	Crossformer	0.6791	3.2933	20.29	0.6278	3.1441	19.89	0.7001	3.4770	37.46	0.6690	3.3048	25.88
	DeformTime	0.7076	3.2300	19.96	0.6311	<u>3.1675</u>	<u>20.08</u>	0.7298	3.4197	37.48	0.6895	<u>3.2724</u>	<u>25.84</u>
	Sonnet	0.7171	3.0995	19.21	0.5982	3.2051	20.27	0.7307	3.3438	37.00	0.6820	3.2161	25.49
120	DLinear	0.5178	4.0071	24.30	0.3307	3.7275	23.27	0.6050	4.1572	43.48	0.4845	3.9640	30.35
	iTransformer	0.5382	3.9632	23.80	0.5504	3.4798	22.72	0.5855	4.1123	44.57	0.5581	3.8518	30.36
	PatchTST	0.3849	4.5359	27.91	0.3942	3.9432	25.12	0.5567	4.2240	44.16	0.4453	4.2344	32.40
	TimeXer	0.6451	3.4743	21.42	0.4839	3.5218	22.15	0.6744	3.9711	42.00	0.6011	3.6557	28.52
	Samformer	0.5761	3.8839	24.10	0.4873	3.6875	23.55	0.6481	3.9545	43.31	0.5705	3.8420	30.32
	ModernTCN	0.5646	3.7511	22.77	0.5422	3.5645	23.40	0.5976	4.2146	43.60	0.5682	3.8434	29.92
	Crossformer	0.6996	3.3054	20.39	0.6396	3.0820	19.72	0.6691	3.7933	40.13	0.6694	3.3935	26.75
	DeformTime	0.7277	3.1270	19.63	0.6141	3.1808	20.31	0.7058	<u>3.5842</u>	<u>38.58</u>	<u>0.6826</u>	<u>3.2973</u>	<u>26.17</u>
	Sonnet	0.7281	3.1081	19.38	0.6365	3.1281	20.03	0.6899	3.5029	38.04	0.6849	3.2464	25.82

Table S4: WEA forecasting results (temperature at 850 hPa) in London (WEA-LD). We assess performance on 3 test periods (years 2016, '17, '18) using linear correlation (r), MAE, and sMAPE ($\epsilon\%$). Best results are **bolded**, second best underlined.

is modelled separately, using its own historical values for prediction. Based on our evaluation, DLinear is the worst-performing model in MTS forecasting. It does not outperform persistence in most experiments (Table 1). This corroborates findings in related work (Shu and Lampos 2025).

Naïve forecasting models. We include simple baseline models as reference points for performance comparison. We use either seasonal persistence or standard persistence, depending on whether a target variable (and task) is characterised by strong seasonality or not. A standard persistence model (naïve baseline) uses the last observed value of the target variable as the prediction (forecasting outcome). The seasonal persistence model uses the value from the same point in the previous seasonal cycle. In our case, the electricity consumption data (ELEC) has a strong seasonal trend, with seasonal persistence outperforming the standard one by a large margin (results not shown). Therefore, we use the seasonal persistence model for the ELEC task, while for the other tasks, we retain standard persistence.

C.2 Additional information on adapting baseline models for Multivariable forecasting tasks

Amongst the selected baselines, DeformTime (Shu and Lampos 2025) and TimeXer (Wang et al. 2024b) are specifically designed for multivariable forecasting tasks. For the rest of the models that were designed for multivariate forecasting, we follow the adaptation strategy from DeformTime and TimeXer, which conduct multivariate forecasting and evaluate the model performance on the target variable. Given that DeformTime and TimeXer have demonstrated their effectiveness across a wide range of forecasting benchmarks, we believe this evaluation provides a fair and consistent comparison against SOTA multivariate forecasting models.

C.3 Attention mechanisms used for time series forecasting

Variable Deformable Attention Block (VDAB). Introduced in DeformTime (Shu and Lampos 2025), VDAB adaptively attends to relevant information across time and variables by applying cross attention over the original and deformed input. This enables to capture complex inter-variable dependencies

H	Model	2016			2017			2018			Average		
		r	MAE	$\epsilon\%$									
4	DLinear	0.9285	1.9481	16.49	0.9182	2.1349	21.52	0.9320	1.8516	15.65	0.9262	1.9782	17.88
	iTransformer	0.9476	1.5907	12.82	0.9412	1.7162	17.87	0.9488	1.5129	12.53	0.9459	1.6066	14.40
	PatchTST	0.9038	2.1592	17.66	0.8927	2.3817	23.79	0.9148	1.9524	16.26	0.9038	2.1644	19.24
	TimeXer	0.9402	1.7540	14.49	0.9382	1.8287	18.59	0.9460	1.6045	13.63	0.9415	1.7290	15.57
	Samformer	0.9478	1.5838	13.06	0.9415	1.7441	17.92	0.9520	1.4729	12.35	0.9471	1.6003	14.44
	ModernTCN	0.9607	1.3723	11.37	0.9539	1.5332	15.92	0.9614	1.3408	11.57	0.9587	1.4154	12.95
	Crossformer	0.9676	1.2417	10.31	0.9631	1.3846	15.29	0.9687	1.2541	11.14	0.9665	1.2935	12.24
	DeformTime	0.9580	1.4031	11.30	0.9592	1.4651	15.92	0.9638	1.3403	11.85	0.9603	1.4028	13.03
	Sonnet	0.9677	<u>1.2506</u>	<u>10.43</u>	0.9645	1.3370	14.70	0.9691	1.2271	10.69	0.9671	1.2716	11.94
12	DLinear	0.8464	2.8374	22.86	0.8060	3.1841	29.99	0.8487	2.8307	23.01	0.8337	2.9507	25.29
	iTransformer	0.8626	2.5160	20.10	0.8275	2.9724	29.06	0.8638	2.4942	20.12	0.8513	2.6609	23.09
	PatchTST	0.8405	2.7056	21.91	0.7976	3.2096	30.96	0.8471	2.6623	21.56	0.8284	2.8592	24.81
	TimeXer	0.8686	2.4893	19.91	0.8404	2.9183	27.85	0.8744	2.5534	20.79	0.8611	2.6537	22.85
	Samformer	0.8646	2.5356	20.66	0.8293	2.9936	29.05	0.8594	2.5914	20.98	0.8511	2.7069	23.57
	ModernTCN	0.8677	2.4940	20.69	0.8332	2.9126	28.23	0.8689	2.4598	19.87	0.8566	2.6221	22.93
	Crossformer	0.8893	2.3005	18.45	0.8570	2.7562	26.36	0.8916	2.2916	<u>18.52</u>	0.8793	2.4494	21.11
	DeformTime	0.8852	<u>2.3050</u>	<u>18.55</u>	<u>0.8519</u>	2.7148	26.08	0.8864	2.3162	18.48	0.8745	2.4453	21.04
	Sonnet	0.8858	2.3262	18.74	0.8499	2.7186	26.25	0.8902	2.2980	18.71	0.8753	2.4476	21.23
28	DLinear	0.8127	3.1132	24.71	0.7533	3.4967	32.30	0.8217	3.0198	24.19	0.7959	3.2099	27.07
	iTransformer	0.8227	2.8172	21.76	0.7710	3.5240	32.26	0.8387	2.7201	21.89	0.8108	3.0204	25.30
	PatchTST	0.8167	2.9402	23.82	0.7579	3.4486	33.28	0.8256	2.8982	23.92	0.8000	3.0956	27.01
	TimeXer	0.8333	2.8010	22.43	0.8052	3.2027	30.03	0.8541	2.6288	20.97	0.8309	2.8775	24.48
	Samformer	0.8221	2.8725	23.07	0.7663	3.3700	32.19	0.8285	2.8616	23.29	0.8056	3.0347	26.18
	ModernTCN	0.8365	2.7179	21.53	0.7673	3.3990	32.94	0.8474	2.6840	21.66	0.8170	2.9336	25.37
	Crossformer	0.8602	2.5428	20.23	0.8107	3.1558	29.80	0.8563	2.6502	20.96	0.8424	2.7830	23.66
	DeformTime	0.8636	2.5246	19.87	<u>0.8166</u>	<u>3.0717</u>	28.77	0.8548	2.6388	20.96	<u>0.8450</u>	<u>2.7450</u>	<u>23.20</u>
	Sonnet	0.8545	2.5533	20.23	0.8342	2.9812	29.08	0.8719	2.4887	19.99	0.8535	2.6744	23.10
120	DLinear	0.7883	3.4169	26.88	0.6870	3.9611	34.99	0.7596	3.4606	27.39	0.7450	3.6129	29.75
	iTransformer	0.8418	2.7846	22.62	0.7691	3.5547	37.41	0.8123	2.9695	23.20	0.8078	3.1029	27.74
	PatchTST	0.7964	3.1199	24.02	0.7451	3.6650	34.57	0.7857	3.4409	27.76	0.7757	3.4086	28.78
	TimeXer	0.8198	2.9056	23.44	0.8003	3.2102	30.24	0.7830	3.3346	25.97	0.8010	3.1501	26.55
	Samformer	0.7795	3.3766	28.57	0.7268	3.9559	42.16	0.7942	3.2543	28.30	0.7668	3.5289	33.01
	ModernTCN	0.7883	3.1432	24.11	0.7353	3.5156	34.01	0.7781	3.2413	26.02	0.7672	3.3000	28.05
	Crossformer	0.8382	2.7770	21.74	0.8143	3.1789	29.76	0.8129	2.9286	22.59	0.8218	2.9615	24.69
	DeformTime	0.8642	2.5570	20.65	0.8013	3.2431	30.09	<u>0.8529</u>	<u>2.6672</u>	<u>20.85</u>	<u>0.8395</u>	<u>2.8224</u>	<u>23.86</u>
	Sonnet	0.8614	2.5606	20.76	0.8377	2.9614	28.01	0.8597	2.6185	20.68	0.8529	2.7135	23.15

Table S5: WEA forecasting results (temperature at 850 hPa) in New York (WEA-NY). We assess performance on 3 test periods (years 2016, '17, '18) using linear correlation (r), MAE, and sMAPE ($\epsilon\%$). Best results are **bolded**, second best underlined.

in MTS forecasting.

Frequency Enhanced Decomposition (FED). Employed in FEDformer (Zhou et al. 2022a), FED decomposes time series into trend and seasonal components, applying attention mechanisms to each, thereby capturing both periodic patterns and time-delay dependencies effectively. We note that we do not compare to the complete forecasting model of FEDformer as it has been outperformed by most of our selected baseline models. Crossformer, iTransformer, PatchTST, ModernTCN, DLinear, and Samformer have all provided direct comparison with FEDformer in their original papers. Meanwhile, the ones that do not provide a direct comparison with FEDformer, namely TimeXer and DeformTime, have both outperformed PatchTST and iTransformer on MTS forecasting tasks by a large margin. Given Sonnet’s competitive performance over all the aforementioned (baseline) models, we expect it to yield superior performance compared to FEDformer.

FNet. The attention proposed in FNet (Lee-Thorp et al. 2022) replaces the commonly used self-attention mechanism in a transformer with a parameter-free Fourier transform. Specifically, it maps the input sequence to the frequency domain

and retains only the real part of the result. This approach enables effective mixing between input tokens along the time dimension without adding learnable parameters. FNet is not included as a baseline model in the main results as it is not a model designed for forecasting purposes. Additionally, we show in Sections 4.3 and 4.4 that it gives a similar performance to the vanilla transformer, which has been outperformed.

Naïve Attention. The commonly used attention module was first proposed by Vaswani et al. (2017) as a core component of the transformer model. The attention weights are computed using scaled dot product operations between query and key embeddings, facilitating the model’s ability to focus on relevant parts of the input sequence.

D Supplementary experiment settings

This section supplements Section 4.1 in the main paper. All experiments were conducted using a Linux server (Ubuntu 24.04.2) with 3 NVIDIA L40S GPUs, 2 AMD EPYC 9354 CPUs, and 768GB of DDR5 RAM, except for the ablation experiments which were conducted using a Linux server

H	Model	2016			2017			2018			Average		
		r	MAE	$\epsilon\%$									
4	DLinear	0.8955	1.0544	7.13	0.9249	0.9475	5.29	0.9091	0.9675	6.21	0.9098	0.9898	6.21
	iTransformer	0.9343	0.8432	5.80	0.9462	0.7692	4.25	0.9404	0.8020	5.20	0.9403	0.8048	5.08
	PatchTST	0.8489	1.2284	8.28	0.8955	1.0634	5.87	0.8612	1.1546	7.31	0.8686	1.1488	7.15
	TimeXer	0.9350	0.9353	6.53	0.9452	0.8258	4.63	0.9515	0.8333	5.41	0.9439	0.8648	5.52
	Samformer	0.9340	0.8454	5.82	0.9455	0.7852	4.32	0.9414	0.7984	5.15	0.9403	0.8097	5.10
	ModernTCN	0.9549	0.7132	4.93	0.9589	0.6858	3.77	0.9551	0.7023	4.57	0.9563	0.7004	4.42
	Crossformer	0.9573	0.6755	4.67	0.9654	0.6245	3.46	0.9628	0.6463	4.19	0.9618	0.6488	4.11
	DeformTime	0.9554	0.7276	5.03	0.9626	0.6519	3.61	0.9620	0.6617	4.31	0.9600	0.6804	4.32
	Sonnet	0.9617	0.6666	4.63	0.9677	<u>0.6253</u>	3.45	0.9673	0.6249	4.08	0.9656	0.6389	4.05
12	DLinear	0.7259	1.6528	11.11	0.8036	1.4281	7.90	0.7237	1.5581	9.85	0.7511	1.5464	9.62
	iTransformer	0.7632	1.5487	10.49	0.8319	1.3230	7.29	0.7864	1.3958	8.80	0.7938	1.4225	8.86
	PatchTST	0.7110	1.6836	11.32	0.7943	1.4387	7.87	0.6995	1.6251	10.11	0.7349	1.5825	9.77
	TimeXer	0.7916	1.4408	9.70	0.8623	1.2177	6.75	0.8406	1.2495	7.94	0.8315	1.3027	8.13
	Samformer	0.7804	1.5051	10.18	0.8340	1.3189	7.28	0.7891	1.3778	8.65	0.8012	1.4006	8.70
	ModernTCN	0.7819	1.4543	9.81	0.8482	1.2875	7.12	0.8026	1.3248	8.35	0.8109	1.3555	8.43
	Crossformer	0.7613	1.4767	9.95	0.8716	1.1834	6.57	<u>0.8463</u>	<u>1.2087</u>	<u>7.73</u>	0.8264	1.2896	8.08
	DeformTime	0.8084	1.4218	9.50	<u>0.8780</u>	<u>1.1443</u>	6.38	0.8351	1.2698	8.09	<u>0.8405</u>	<u>1.2786</u>	7.99
	Sonnet	0.8114	1.3921	9.35	0.8820	1.1220	6.25	0.8548	1.1923	7.62	0.8494	1.2355	7.74
28	DLinear	0.6844	1.6762	11.32	0.7547	1.5545	8.56	0.6757	1.6389	10.30	0.7049	1.6232	10.06
	iTransformer	0.6986	1.6872	11.39	0.7499	1.6095	8.79	0.6914	1.6101	10.07	0.7133	1.6356	10.08
	PatchTST	0.6935	1.6950	11.50	0.7515	1.5721	8.64	0.6758	1.6653	10.34	0.7069	1.6441	10.16
	TimeXer	0.7459	1.5904	10.71	0.8013	1.4330	7.92	0.7581	1.5111	9.55	0.7684	1.5115	9.39
	Samformer	0.6904	1.6976	11.49	0.7735	1.5271	8.43	0.6872	1.6431	10.25	0.7170	1.6226	10.05
	ModernTCN	0.6928	1.7091	11.51	0.7954	1.4720	8.06	0.7131	1.5787	9.89	0.7338	1.5866	9.82
	Crossformer	0.6899	1.7047	11.32	0.8231	1.4059	7.75	0.7642	1.4739	9.29	0.7590	1.5282	9.45
	DeformTime	0.7721	1.5560	10.36	0.8288	1.3821	7.67	0.7724	1.4858	9.44	0.7911	1.4746	9.16
	Sonnet	0.7714	1.5099	10.11	0.8518	1.2950	7.22	0.7718	1.4355	9.16	0.7983	1.4135	8.83
120	DLinear	0.6432	1.9457	13.25	0.6875	1.8548	10.28	0.7085	1.6983	10.94	0.6797	1.8329	11.49
	iTransformer	0.7564	1.6063	11.01	0.7150	1.6955	9.34	0.6740	1.7218	10.98	0.7152	1.6745	10.45
	PatchTST	0.6846	2.1676	15.78	0.6216	2.0684	11.43	0.7092	1.7893	11.30	0.6718	2.0084	12.84
	TimeXer	0.7208	1.7303	11.64	0.6869	1.7013	9.33	0.7211	1.6961	10.69	0.7096	1.7092	10.55
	Samformer	0.6898	1.9304	13.80	0.6868	1.8838	10.46	0.7217	1.8388	11.93	0.6995	1.8843	12.06
	ModernTCN	0.7470	1.6455	11.27	<u>0.7985</u>	1.5017	8.31	0.6635	1.7506	11.09	0.7363	1.6326	10.22
	Crossformer	0.6789	1.7296	11.34	0.7945	1.4771	8.09	0.7373	1.5724	9.77	0.7369	1.5931	9.73
	DeformTime	0.7630	<u>1.6101</u>	10.65	0.7953	1.5073	8.23	<u>0.7459</u>	<u>1.5023</u>	<u>9.46</u>	<u>0.7681</u>	1.5399	9.45
	Sonnet	0.7563	1.7449	11.65	0.8106	1.4349	7.92	0.7739	1.4610	9.17	0.7803	<u>1.5469</u>	<u>9.58</u>

Table S6: WEA forecasting results (temperature at 850 hPa) in Hong Kong (WEA-HK). We assess performance on 3 test periods (years 2016, '17, '18) using linear correlation (r), MAE, and sMAPE ($\epsilon\%$). Best results are **bolded**, second best underlined.

(Ubuntu 22.04.5) with 2 NVIDIA A40 GPUs, 2 AMD EPYC 7443 CPUs, and 512GB of DDR4 RAM.

D.1 Hyperparameter settings

The look-back window L is set differently depending on the forecasting task. For the ETTh1, ETTh2 data sets, L is set to 336 time steps for all 4 different forecasting horizons $H = \{96, 192, 336, 720\}$, based on prior work (Nie et al. 2023). In ELEC experiments, we set $L = 168$ hours (a week, given the strong weekly periodicity in these time series) for all $H = \{12, 24, 36\}$. For ENER, L is set equal to the forecasting horizon, i.e. $L = H = \{24, 48, 72, 168\}$. For the WEA tasks, we use a look-back window $L = \{28, 28, 56, 240\}$ time steps for $H = \{4, 12, 28, 120\}$, correspondingly. This means that we use the past 7 days to conduct short-term forecasts (1 and 3 days ahead), and the past $2H$ days for longer-term forecasts. For the ILI tasks, we set $L = \{28, 28, 56, 56\}$ days respectively for forecasting horizons $H = \{7, 14, 21, 28\}$ days ahead following prior work (Shu and Lampos 2025).

The batch size d is set to 64 for all tasks except for the ETT ones, where it is a learnable hyperparameter (see section D.4).

We train using a maximum of 100 epochs (see our early stopping settings in D.4). Neural networks are optimised with Adam using mean squared error (MSE) loss on all time steps. Note that the output can be a time series (sequence) of one variable (the target) or more variables (target and exogenous), depending on the forecasting method.

D.2 Hyperparameter settings specific to Sonnet

For Sonnet, the parameter α that controls the dimensionality of the embeddings of the endo- and exogenous variables is chosen from $\alpha \in \{0, .1, .25, .75\}$. The number of atoms, K , is selected from the set $K \in \{8, 16, 32\}$. The hidden dimension d of Sonnet is set to be 64.

D.3 Hyperparameter settings specific to the ILI rate forecasting tasks

In the ILI rate forecasting task, the number of exogenous variables is decided using a learnable threshold τ based on linear correlation (with the endogenous/target variable in the training data), following DeformTime (Shu and Lampos 2025). We select τ from $\{.3, .4, .5\}$ for the US regions, and

H	Model	2016			2017			2018			Average		
		r	MAE	$\epsilon\%$									
4	DLinear	0.7760	0.4068	1.47	0.7495	0.4174	1.52	0.7885	0.3903	1.43	0.7713	0.4048	1.47
	iTransformer	0.8033	0.3835	1.38	0.7777	0.3985	1.45	0.8089	0.3783	1.39	0.7967	0.3868	1.41
	PatchTST	0.7572	0.4194	1.51	0.7266	0.4364	1.59	0.7578	0.4156	1.53	0.7472	0.4238	1.54
	TimeXer	0.7933	0.3910	1.41	0.8010	0.3780	1.38	0.8147	0.3712	1.36	0.8030	0.3801	1.38
	Samformer	0.7917	0.3940	1.42	0.7690	0.4064	1.48	0.8109	0.3770	1.38	0.7905	0.3925	1.43
	ModernTCN	0.8194	<u>0.3664</u>	<u>1.32</u>	0.8135	0.3662	1.34	0.8286	0.3546	1.30	0.8205	0.3624	1.32
	Crossformer	0.8198	0.3695	1.33	0.8403	0.3441	1.26	0.8407	0.3462	1.27	<u>0.8336</u>	<u>0.3532</u>	<u>1.29</u>
	DeformTime	0.8166	0.3737	1.35	0.8356	0.3452	1.26	0.8349	0.3481	1.28	0.8290	0.3557	1.30
	Sonnet	0.8313	0.3564	1.29	<u>0.8363</u>	0.3431	1.25	0.8469	0.3336	1.22	0.8382	0.3444	1.25
12	DLinear	0.6873	0.4789	1.72	0.6565	0.4844	1.77	0.6639	0.4658	1.71	0.6693	0.4764	1.73
	iTransformer	0.7134	0.4571	1.65	0.6811	0.4714	1.72	0.6759	0.4702	1.72	0.6901	0.4662	1.70
	PatchTST	0.6632	0.4880	1.76	0.6201	0.5099	1.86	0.6236	0.4995	1.83	0.6356	0.4992	1.82
	TimeXer	0.7178	0.4516	1.63	0.7203	0.4404	1.61	0.7084	0.4421	1.62	0.7155	0.4447	1.62
	Samformer	0.6976	0.4696	1.69	0.6613	0.4875	1.78	0.6680	0.4779	1.75	0.6756	0.4784	1.74
	ModernTCN	0.7328	0.4458	1.61	0.7179	0.4445	1.62	0.7022	0.4576	1.68	0.7177	0.4493	1.64
	Crossformer	0.7326	0.4548	1.64	<u>0.7615</u>	0.4124	1.50	0.7283	0.4406	1.61	<u>0.7408</u>	0.4359	1.59
	DeformTime	<u>0.7336</u>	<u>0.4319</u>	<u>1.56</u>	0.7551	0.4203	1.53	<u>0.7325</u>	<u>0.4246</u>	<u>1.56</u>	<u>0.7404</u>	<u>0.4256</u>	<u>1.55</u>
	Sonnet	0.7456	0.4302	1.55	0.7752	0.4009	1.46	0.7437	0.4169	1.53	0.7548	0.4160	1.51
28	DLinear	0.6046	0.5229	1.88	0.5531	0.5403	1.97	0.5513	0.5220	1.92	0.5697	0.5284	1.92
	iTransformer	0.5986	0.5261	1.90	0.5899	0.5339	1.95	0.5652	0.5322	1.95	0.5846	0.5307	1.93
	PatchTST	0.5614	0.5468	1.97	0.5414	0.5593	2.04	0.5210	0.5566	2.04	0.5413	0.5542	2.02
	TimeXer	0.6816	0.4966	1.79	0.6231	0.5027	1.83	0.6152	0.4930	1.81	0.6399	0.4974	1.81
	Samformer	0.5995	<u>0.5262</u>	1.90	0.5566	0.5498	2.00	0.5384	0.5503	2.02	0.5648	0.5421	1.97
	ModernTCN	0.6151	0.5183	1.87	0.6013	0.5186	1.89	0.5871	0.5220	1.92	0.6012	0.5196	1.89
	Crossformer	0.6660	0.5212	1.88	0.6690	0.5088	1.85	0.6692	0.4711	1.73	<u>0.6681</u>	0.5003	1.82
	DeformTime	0.6705	0.5058	1.82	0.6664	<u>0.4869</u>	1.78	0.6638	<u>0.4698</u>	<u>1.72</u>	0.6669	<u>0.4875</u>	<u>1.77</u>
	Sonnet	0.7098	0.4605	1.66	0.6890	0.4721	1.72	0.6856	0.4633	1.70	0.6948	0.4653	1.69
120	DLinear	0.6260	0.5535	1.99	0.4837	0.5678	2.07	0.6341	<u>0.4773</u>	<u>1.75</u>	0.5812	0.5328	1.94
	iTransformer	0.6079	0.5563	2.00	0.6114	0.5013	1.83	0.5811	0.5124	1.88	0.6001	0.5233	1.90
	PatchTST	0.6435	<u>0.5017</u>	<u>1.81</u>	0.4324	0.6084	2.22	0.6099	0.4972	1.82	0.5619	0.5357	1.95
	TimeXer	0.6139	0.5558	2.00	0.6150	0.5044	1.84	0.5935	0.5042	1.85	0.6075	0.5215	1.90
	Samformer	0.5653	0.5537	2.00	0.5719	0.5212	1.90	0.6136	0.4914	1.80	0.5836	0.5221	1.90
	ModernTCN	0.6442	0.5410	1.95	0.5708	0.5321	1.94	0.5764	0.5233	1.92	0.5971	0.5321	1.94
	Crossformer	<u>0.6500</u>	0.5573	2.00	0.6383	0.5133	1.87	0.6498	0.4929	1.81	<u>0.6461</u>	0.5212	1.89
	DeformTime	0.6204	0.5384	1.94	0.6661	<u>0.4815</u>	<u>1.75</u>	0.6308	0.4951	1.81	0.6391	<u>0.5050</u>	<u>1.83</u>
	Sonnet	0.6609	0.5005	1.80	<u>0.6583</u>	0.4794	1.75	0.6568	0.4692	1.72	0.6587	0.4830	1.76

Table S7: WEA forecasting results (temperature at 850 hPa) in Singapore (WEA-SG). We assess performance on 3 test periods (years 2016, '17, '18) using linear correlation (r), MAE, and sMAPE ($\epsilon\%$). Best results are **bolded**, second best underlined.

from $\{.05, .1, .2, .3, .4, .5\}$ for England. An increase in the correlation threshold leads to a reduction in the number of selected queries. Consequently, the number of search queries selected by the models ranges from 13 to 51 for US regions, and from 80 to 752 for England. For the models that require an excessive amount of GPU memory for larger sets of exogenous variables, i.e. ModernTCN, PatchTST and Crossformer, we restricted $\tau \in \{.3, .4, .5\}$ for all regions.

D.4 Hyperparameter validation

For the ETT forecasting tasks, the batch size and the hidden dimension d are both selected from $\{16, 32, 64\}$. For all tasks, Adam's initial learning rate is selected from $\{2, 1, .5, .2, .1, .05\} \times 10^{-3}$. The learning rate is decayed to 0 with a linear decay scheduler applied after every epoch. If a model structure contains a dropout parameter, its value is selected from $\{0, .1, .2\}$. Hyperparameter values are determined using grid search. Training stops early when the validation error of the target variable over time $\{t+1, \dots, t+H\}$ does not decrease further (compared to its lowest value) for 5 consecutive epochs. We then use the model with the lowest

validation loss.

D.5 Data normalisation

We apply z-score normalisation to the data of all forecasting tasks. This standardises endogenous and exogenous variables in a training set to have a zero mean and unit standard deviation. Normalisation is transferred from the training data to the test data. Data is reverted back to the original scale when computing prediction errors. Additionally, for the ETT, ENER, and ELEC data sets, we adopt variable normalisation (Kim et al. 2022) over the target variable within the input's look-back window following prior work (Nie et al. 2023; Shu and Lampos 2025).

D.6 sMAPE definition for the weather (temperature) prediction tasks

We note that for the WEA tasks, the unit of the temperature time series sequence is originally captured in Kelvin.¹⁰ Directly computing the sMAPE using Kelvin units will lead to

¹⁰0 degrees in Celsius is equal to 273.15 Kelvin.

H	Model	2016			2017			2018			Average		
		r	MAE	$\epsilon\%$									
4	DLinear	0.6899	3.0696	17.69	0.6677	3.3553	19.03	0.6757	3.0199	17.93	0.6778	3.1483	18.22
	iTransformer	0.8466	2.1083	12.25	0.8325	2.3752	13.70	0.8464	2.0884	12.54	0.8418	2.1906	12.83
	PatchTST	0.5931	3.3676	19.33	0.5788	3.7192	21.07	0.5372	3.4144	20.12	0.5697	3.5004	20.17
	TimeXer	0.8464	2.1310	12.48	0.8412	2.4309	13.92	0.8407	2.1510	13.03	0.8428	2.2376	13.14
	Samformer	0.8495	2.0911	12.19	0.8248	2.4305	14.03	0.8338	2.1580	13.04	0.8361	2.2265	13.09
	ModernTCN	0.8955	1.7858	10.42	0.8852	1.9753	11.44	0.8806	1.8644	11.30	0.8871	1.8752	11.05
	Crossformer	0.9114	1.5785	9.13	0.9070	1.7736	10.34	0.9135	1.5626	9.38	0.9106	1.6382	9.62
	DeformTime	0.9044	1.7005	9.98	0.8880	1.9208	11.12	0.9057	1.6589	10.15	0.8994	1.7600	10.41
	Sonnet	0.9169	1.5732	<u>9.20</u>	<u>0.9068</u>	1.7550	10.26	0.9160	1.5439	<u>9.42</u>	0.9133	1.6240	<u>9.63</u>
12	DLinear	0.3597	3.9731	22.60	0.3874	4.1974	23.32	0.3239	3.9091	22.89	0.3570	4.0265	22.94
	iTransformer	0.4321	3.8589	22.11	0.4092	4.2382	23.80	0.3857	3.8253	22.58	0.4090	3.9741	22.83
	PatchTST	0.3525	4.1364	23.67	0.3792	4.3989	24.52	0.3214	4.0377	23.78	0.3511	4.1910	23.99
	TimeXer	0.4979	3.6755	20.94	0.4804	3.9628	22.14	0.4763	3.5340	20.86	0.4849	3.7241	21.31
	Samformer	0.4245	3.9482	22.49	0.4137	4.2929	23.97	0.3626	3.8921	22.95	0.4003	4.0444	23.14
	ModernTCN	0.4861	3.6737	21.11	0.4560	4.0876	22.78	0.4537	3.5671	21.10	0.4653	3.7761	21.67
	Crossformer	0.5485	3.5536	20.27	0.5238	3.8275	21.42	0.5246	3.3985	20.16	0.5323	3.5932	20.62
	DeformTime	0.5377	3.5610	20.29	<u>0.5394</u>	<u>3.7613</u>	<u>21.00</u>	<u>0.5267</u>	<u>3.3821</u>	<u>20.10</u>	<u>0.5346</u>	<u>3.5681</u>	<u>20.46</u>
	Sonnet	0.5527	3.5423	<u>20.27</u>	0.5452	3.7261	20.89	0.5389	3.3613	19.99	0.5456	3.5432	20.38
28	DLinear	0.3869	3.9030	22.17	0.4155	4.1227	22.99	0.4047	3.7504	21.94	0.4024	3.9254	22.37
	iTransformer	0.3651	4.0092	22.90	0.4111	4.1308	23.10	0.4143	3.7352	21.79	0.3969	3.9584	22.60
	PatchTST	0.3824	3.9671	22.57	0.4173	4.1099	23.01	0.4097	3.7444	21.86	0.4031	3.9405	22.48
	TimeXer	0.4448	3.8264	21.80	0.5026	3.9775	22.20	0.4052	3.6936	21.60	0.4509	3.8325	21.87
	Samformer	0.3968	3.9169	22.27	0.4159	4.1299	23.09	0.4219	3.7249	21.76	0.4116	3.9239	22.37
	ModernTCN	0.3972	3.9191	22.28	0.3855	4.2644	23.63	<u>0.4480</u>	3.6363	21.18	0.4102	3.9399	22.36
	Crossformer	0.4491	3.8314	21.83	0.4861	3.9413	22.02	0.4135	3.6457	21.32	0.4495	3.8061	21.72
	DeformTime	0.4704	3.7845	<u>21.60</u>	0.4990	3.9476	22.06	0.4510	3.5481	20.82	<u>0.4735</u>	<u>3.7601</u>	<u>21.49</u>
	Sonnet	0.4829	3.7430	21.39	0.5017	3.8840	21.73	0.4436	3.5560	20.84	0.4761	3.7277	21.32
120	DLinear	0.2564	4.1508	23.51	0.4413	4.0823	22.74	0.2488	3.9379	22.90	0.3155	4.0570	23.05
	iTransformer	0.3760	4.0470	22.88	0.4466	3.9902	22.30	0.3580	3.8046	22.30	0.3935	3.9473	22.49
	PatchTST	0.3485	4.0798	23.27	0.4448	4.0213	22.37	0.2282	4.0629	23.42	0.3405	4.0547	23.02
	TimeXer	0.4334	3.8432	21.84	0.4717	4.0044	22.36	0.4079	3.6759	21.44	0.4377	3.8412	21.88
	Samformer	0.3890	4.0904	23.47	0.4684	3.9402	21.96	0.3858	3.6749	21.47	0.4144	3.9018	22.30
	ModernTCN	0.4450	3.9583	22.94	0.4212	4.1221	23.01	0.2811	4.1861	24.68	0.3824	4.0889	23.54
	Crossformer	0.4738	3.7648	21.45	0.5259	3.8475	21.54	0.3787	3.6852	21.49	0.4595	3.7659	21.49
	DeformTime	0.4758	<u>3.7615</u>	<u>21.44</u>	0.4537	3.9905	22.23	0.3999	<u>3.6602</u>	<u>21.34</u>	0.4431	3.8040	21.67
	Sonnet	0.4718	3.7594	21.41	<u>0.5126</u>	<u>3.9088</u>	<u>21.86</u>	0.4389	3.5438	20.79	0.4744	3.7373	21.35

Table S8: WEA forecasting results (temperature at 850 hPa) in Cape Town (WEA-CT). We assess performance on 3 test periods (years 2016, '17, '18) using linear correlation (r), MAE, and sMAPE ($\epsilon\%$). Best results are **bolded**, second best underlined.

a relatively small error (MAEs are not affected, but sMAPEs will be significantly lower and harder to display in an accessible way). To address this, we subtract the minimum value of the target variable across the test set ($\xi = \min(\mathbf{y})$), and then add a constant number $a = 30$ to both the ground truth and the predicted value to avoid division by 0. This alters the formula of sMAPE as follows:

$$\text{sMAPE}(\mathbf{y}, \hat{\mathbf{y}}) = \frac{100}{L} \sum_{t=1}^L \frac{2|y_t - \hat{y}_t|}{(|y_t - \xi| + |\hat{y}_t - \xi| + 2a)}. \quad (\text{S1})$$

D.7 Random seed initialisation

We use a fixed seed equal to '42' during training for all forecasting tasks, except for the ETTh1 and ETTh2 data sets. For these data sets, we follow prior work (Nie et al. 2023; Zeng et al. 2023) and use '2021', with the exception of iTransformer, which uses '2023' in line with its official configuration.

D.8 Replacing attention modules with MVCA

To use MVCA in place of vanilla attention in the 3 base models for experiments in Section 4.3, some modifications are

needed as MVCA initially expects a 3-dimensional input in $\mathbb{R}^{K \times L \times d}$ with K as the number of wavelet transformations (which we use as the number of heads in multi-head MVCA). In contrast, the attention module in the three base models takes input embeddings with only 2 dimensions $\in \mathbb{R}^{u \times v}$, which represent time and variables. To address this discrepancy, we split the embedding into multiple attention heads, as MVCA is essentially a variant similar to multihead attention. Specifically, given an embedding in shape $\mathbb{R}^{u \times v}$, we first split it along the feature dimension into K heads, resulting in an input dimension of v/K for each head, where the head embeddings are in shape $\mathbb{R}^{K \times u \times (v/K)}$. The remaining operations then follow the standard MVCA process, with u and v/K corresponding to L and d respectively. The output of different heads is also joined along the feature dimension to form the final output in shape $\mathbb{R}^{u \times v}$. In our experiment, the number of heads is fixed to 8 for all base models when replacing the attention with MVCA.

E Supplementary results

This section supplements section 4 of the main paper.

Model	Variant	$H=7$			$H=14$			$H=21$			$H=28$		
		ENG	US2	US9									
iTransformer	—	26.38	23.24	18.57	36.67	28.17	22.44	48.93	30.03	24.11	55.35	36.75	31.05
	\neg Attn	26.22	25.52	21.22	37.10	30.54	25.77	54.52	34.77	29.89	61.97	41.18	34.97
	FNet (2022)	30.16	26.99	22.27	41.28	31.12	26.29	57.16	36.48	29.69	64.26	41.06	35.00
	FED (2022a)	40.21	32.58	26.25	48.37	37.86	30.68	67.76	50.94	40.97	73.86	54.82	44.33
	VDAB (2025)	27.46	24.55	19.21	38.10	30.39	23.29	48.19	32.37	<u>23.07</u>	54.16	35.39	26.97
	MVCA	26.87	20.27	16.34	37.71	26.01	20.77	50.64	27.94	22.19	57.64	33.23	24.89
SamFormer	—	28.31	24.21	19.39	36.63	30.16	24.50	54.41	31.42	24.22	60.78	36.8	27.95
	\neg Attn	29.99	29.26	24.13	40.52	34.58	28.73	52.00	41.77	36.09	62.22	46.08	40.87
	FNet (2022)	30.01	27.94	21.95	40.33	33.06	27.33	53.16	36.21	31.30	61.64	42.28	34.68
	FED (2022a)	40.18	32.35	26.34	48.91	37.65	30.84	67.79	49.99	41.26	73.17	53.91	44.85
	VDAB (2025)	25.98	<u>21.88</u>	<u>17.05</u>	<u>36.84</u>	<u>27.48</u>	20.95	46.52	<u>30.78</u>	22.29	<u>57.09</u>	<u>33.49</u>	<u>25.63</u>
	MVCA	<u>26.13</u>	20.85	16.90	38.14	26.14	<u>21.06</u>	<u>49.15</u>	28.55	<u>22.57</u>	55.27	32.39	24.66
PatchTST	—	27.61	24.51	19.34	37.76	30.11	24.09	51.11	36.70	29.40	<u>59.60</u>	42.61	33.35
	\neg Attn	28.54	26.99	21.51	41.64	31.82	26.36	53.64	38.75	31.75	<u>60.11</u>	43.25	36.17
	FNet (2022)	31.93	28.81	22.14	44.15	33.77	25.64	58.17	38.11	26.46	60.51	41.48	29.92
	FED (2022a)	40.21	32.59	26.25	50.26	37.88	30.76	67.85	50.89	41.16	74.08	54.61	44.42
	VDAB (2025)	<u>26.88</u>	<u>22.99</u>	<u>17.99</u>	38.08	30.99	<u>20.64</u>	<u>50.49</u>	32.45	<u>23.90</u>	60.16	34.89	25.61
	MVCA	25.77	22.90	17.50	<u>37.97</u>	28.33	20.48	49.10	<u>32.45</u>	22.05	59.48	<u>36.14</u>	<u>25.97</u>

Table S9: Performance (average sMAPE across the 4 test seasons) of iTransformer, Samformer, and PatchTST on the ILI forecasting tasks (ILI-ENG/US2/US9) with different modifications to the naïve attention mechanism. ‘ \neg Attn’ denotes the removal of the residual attention module, and FNet / FED / VDAB refer to using the attention modules proposed in FNet, FEDformer, and DeformTime, respectively. This table supplements Table 2. Best results are **bolded**, second best underlined.

E.1 Detailed forecasting results with the ILI and weather forecasting tasks

Complete results, broken down across all test periods, models, and forecasting horizons for the ILI rate prediction tasks in England (ILI-ENG), US Region 2 (ILI-US2), and US Region 9 (ILI-US9) are enumerated in Tables S1, S2, and S3, respectively. Similarly, Tables S4–S8 present the corresponding results for weather forecasting in London (WEA-LD), New York (WEA-NY), Singapore (WEA-SG), Hong Kong (WEA-HK), and Cape Town (WEA-CT). For both tasks, we report MAE, sMAPE ($\epsilon\%$), and the linear correlation coefficient (denoted by r) between the model predictions and the target values over each test period.

E.2 Supplementary experiment results with sMAPE score

Results enumerated in Table S9 complement the ones presented in Section 4.3, Table 2 by providing sMAPE estimates ($\epsilon\%$). On average, replacing the attention in the base models with MVCA reduces sMAPE by 9%. Moreover, compared to the best-performing variant (VDAB), our proposed MVCA reduces sMAPE by 2.3%. This reduction in relative error further consolidates our argument that MVCA provides better prediction accuracy in MTS forecasting.

E.3 Ablation study on Sonnet

An ablation study is performed to better understand the contribution of Sonnet’s components to the overall performance. We ablate over the following modules: the coherence mechanism (within MVCA), the MLP head for inter-variable dependency modelling (within MVCA), the complete MVCA module (section 3.3), the joint embedding module (section 3.1), and the Koopman evolution module (section 3.4).

A detailed description of each ablation variant is provided as follows:

- \neg **Coher**: This denotes that in MVCA, we do not compute the coherence attention. Instead of multiplying the attention with the value embedding ($\mathbf{O}_h = \mathbf{A} \odot \mathbf{V}_h$), the output embedding of each head \mathbf{O}_h is equal to the value embedding, i.e. $\mathbf{O}_h = \mathbf{V}_h$. In this case, the attention highlighting temporal importance is not included; only the MLP that captures the variable dependency is included.
- \neg **MLP**: This denotes that we do not add the residual connection with the two-layer perceptron to obtain the attention output. Instead of computing $\mathbf{O}_m = \mathbf{O}_r + \text{MLP}(\mathbf{O}_r)$, we directly have $\mathbf{O}_m = \mathbf{O}_r$. In this case, the inter-variable dependency via the MLP is omitted. Although some inter-variable interactions are partially (no learnable parameter is included in this process) captured when transforming the input into the frequency space along the feature dimension.
- \neg **MVCA**: This denotes that we remove the MVCA from the modelling structure of Sonnet. After projecting the embedding into the wavelet space using the learnable wavelet transform, we directly feed the input into the Koopman evolution layer.
- \neg **Embed**: This denotes that instead of embedding the endo- and exogenous variables separately with 2 different weight matrices, we use 1 single weight matrix, $\mathbf{W} \in \mathbb{R}^{(C+1) \times d}$, over all input variables, $\mathbf{Z} \in \mathbb{R}^{L \times (C+1)}$, to obtain the input embedding $\mathbf{E} \in \mathbb{R}^{L \times d} = \mathbf{Z}\mathbf{W}$.
- \neg **Koop**: This denotes that we do not predict the next step of the temporal state using the Koopman operator. Instead, after capturing the dependencies using MVCA, the time series is directly reconstructed from the output of the attention module.

We re-tune Sonnet’s hyperparameters for each ablation variant across all locations, test seasons, and forecasting horizons.

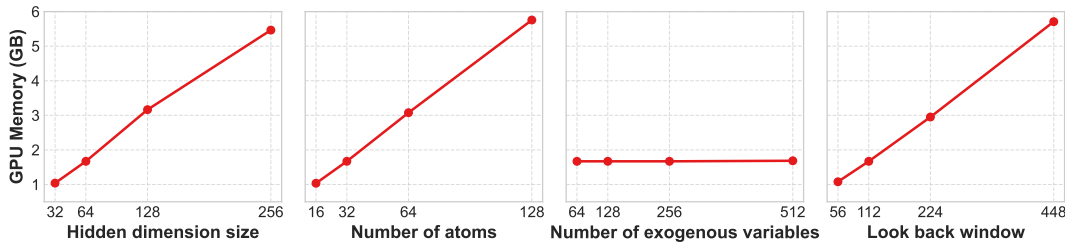


Figure S1: Computational cost (GPU memory) of Sonnet regarding the hidden dimension size d , the number of atoms K , the number of exogenous variables C , and the look back window length L .

zons (for the ILI and WEA tasks).

Results are enumerated in Table S10. We report the average MAE across all test seasons and its percentage of difference compared to the Sonnet model (enumerated in Table 1). Among all the ablated components, the MVCA module has

		\neg Coher	\neg MLP	\neg MVCA	\neg Embed	\neg Koop					
	H	MAE	$\Delta\%$	MAE	$\Delta\%$	MAE	$\Delta\%$	MAE	$\Delta\%$	MAE	$\Delta\%$
ILI-ENG	7	1.422	-3.8	1.531	+3.5	1.591	+7.5	1.633	+10.4	1.486	+0.4
	14	2.110	+9.7	2.171	+12.9	2.235	+16.2	2.066	+7.5	2.079	+8.2
	21	2.880	+14.7	2.614	+4.1	2.794	+11.3	2.647	+5.4	2.630	+4.8
	28	3.420	+24.4	3.114	+13.3	3.274	+19.2	3.091	+12.5	3.062	+11.4
ILI-US2	7	0.414	+8.8	0.411	+8.0	0.432	+13.4	0.416	+9.4	0.420	+10.5
	14	0.512	+14.0	0.507	+13.0	0.528	+17.5	0.530	+17.9	0.496	+10.5
	21	0.609	+14.3	0.596	+12.0	0.671	+26.0	0.573	+7.6	0.590	+10.8
	28	0.623	+7.7	0.662	+14.4	0.666	+15.0	0.606	+4.8	0.634	+9.5
ILI-US9	7	0.272	+1.9	0.302	+13.1	0.277	+4.0	0.278	+4.4	0.280	+4.8
	14	0.318	+13.4	0.334	+19.0	0.331	+17.8	0.315	+12.1	0.315	+12.3
	21	0.358	+12.5	0.326	+2.7	0.393	+23.6	0.311	-2.1	0.319	+0.4
	28	0.428	+16.4	0.345	-6.2	0.401	+9.2	0.359	-2.4	0.348	-5.4
WEA-CT	4	1.663	+2.4	1.643	+1.2	1.636	+0.7	1.678	+3.3	1.650	+1.6
	12	3.591	+1.3	3.574	+0.9	3.589	+1.3	3.572	+0.8	3.568	+0.7
	28	3.783	+1.5	3.760	+0.9	3.862	+3.6	3.765	+1.0	3.754	+0.7
	120	3.769	+0.9	3.764	+0.7	3.768	+0.8	3.766	+0.8	3.767	+0.8
WEA-HK	4	0.639	+0.0	0.639	+0.1	0.631	-1.2	0.655	+2.6	0.639	+0.1
	12	1.290	+4.4	1.261	+2.0	1.302	+5.4	1.278	+3.4	1.273	+3.1
	28	1.475	+4.3	1.467	+3.8	1.477	+4.5	1.467	+3.8	1.463	+3.5
	120	1.635	+5.7	1.627	+5.2	1.620	+4.7	1.599	+3.4	1.604	+3.7
WEA-LD	4	1.754	+1.8	1.767	+2.6	1.742	+1.1	1.787	+3.7	1.755	+1.9
	12	2.991	+1.1	3.007	+1.6	3.001	+1.4	3.019	+2.0	2.993	+1.1
	28	3.313	+3.0	3.281	+2.0	3.328	+3.5	3.326	+3.4	3.268	+1.6
	120	3.385	+4.3	3.347	+3.1	3.375	+4.0	3.359	+3.5	3.345	+3.1
WEA-NY	4	1.296	+1.9	1.294	+1.8	1.281	+0.7	1.316	+3.5	1.284	+1.0
	12	2.447	-0.0	2.464	+0.7	2.468	+0.9	2.467	+0.8	2.460	+0.5
	28	2.751	+2.9	2.708	+1.3	2.764	+3.4	2.739	+2.4	2.723	+1.8
	120	2.856	+5.3	2.777	+2.4	2.938	+8.3	2.840	+4.7	2.801	+3.2
WEA-SG	4	0.342	-0.8	0.345	+0.1	0.343	-0.5	0.348	+1.1	0.343	-0.4
	12	0.423	+1.6	0.419	+0.8	0.426	+2.4	0.423	+1.6	0.422	+1.4
	28	0.489	+5.2	0.476	+2.2	0.474	+1.9	0.475	+2.2	0.476	+2.3
	120	0.500	+3.5	0.494	+2.3	0.503	+4.1	0.497	+2.8	0.495	+2.5

Table S10: Ablation study results across the ILI (4 test seasons) and WEA tasks (3 test years). MAE is shown for each ablated variation (\neg denotes removal of a component). $\Delta\%$ is the MAE percentage of difference compared to Sonnet’s MAE (which can be seen in Table 1). MAE values are rounded to 3 decimals for spacing. Grey background denotes a performance drop (increased MAE) compared to Sonnet.

the greatest impact. Removing MVCA results in an increase of MAE by 6.3% on average across the ILI and WEA tasks. Breaking down MVCA further, we observe that removing its two internal components: coherency modelling and the MLP residual connection, leads to notable drops in performance (5.2% and 4.1% increase in MAE, respectively), but less pronounced than removing the entire MVCA block. This indicates that while capturing coherence over time and enhancing variable interactions with residual connected MLP are both important modules, they also work in tandem within the full MVCA design.

Other components within Sonnet also contribute to the

H	seed	2015/16	2016/17	2017/18	2018/19	Average
7	10	1.088	1.194	1.756	1.490	1.382
	42	1.029	1.200	2.037	1.650	1.479
	111	1.065	1.061	2.070	1.497	1.423
	1111	1.188	1.182	1.815	1.220	1.351
	1234	1.095	1.200	1.974	1.478	1.437
	μ	1.09	1.17	1.93	1.47	1.41
	σ	0.06	0.06	0.14	0.16	0.05
14	10	1.539	1.418	3.022	1.916	1.974
	42	1.533	1.245	2.831	2.081	1.923
	111	1.672	1.623	2.905	2.257	2.114
	1111	1.590	1.492	2.937	2.049	2.017
	1234	1.668	1.545	2.928	1.727	1.967
	μ	1.60	1.46	2.92	2.01	2.00
	σ	0.07	0.14	0.07	0.20	0.07
21	10	1.813	1.524	3.999	2.569	2.476
	42	1.939	1.568	3.971	2.562	2.510
	111	1.945	1.329	3.907	2.541	2.431
	1111	1.966	1.487	4.001	2.469	2.481
	1234	2.107	1.320	4.006	2.542	2.494
	μ	1.95	1.45	3.98	2.54	2.48
	σ	0.10	0.11	0.04	0.04	0.03
28	10	2.324	1.746	4.417	2.986	2.869
	42	2.013	1.749	4.460	2.770	2.748
	111	2.142	1.596	4.346	2.898	2.745
	1111	2.322	1.599	4.606	2.955	2.870
	1234	2.342	1.740	4.191	2.781	2.764
	μ	2.23	1.69	4.40	2.88	2.80
	σ	0.15	0.08	0.15	0.10	0.06

Table S11: Seed control (5 seeds) for Sonnet using the ILI-ENG data set across all forecasting horizons (H). μ and σ denote the mean and standard deviation of the 5 obtained MAEs per test period. The results in the main paper were obtained for seed ‘42’.

model’s predictive ability, although to a lesser extent. Removing the joint embedding module leads to a 4% increase in MAE, highlighting the importance of separately encoding the target and exogenous variables. Additionally, removing the Koopman operator module increases MAE by 3.2%, demonstrating the effectiveness of modelling the temporal evolution. Interestingly, as the forecasting horizon H increases, the performance degradation becomes greater when removing coherence in MVCA, from an MAE increase of 2% and 1.1% (shortest H) for the ILI and WEA tasks, respectively, to 13.6% and 3.7% (longest H). This indicates that spectral coherence is more important for longer-term forecasting.

E.4 Sensitivity to random seed initialisation

Results that assess the sensitivity of Sonnet to different random seed initialisations are enumerated in Table S11. We have examined 5 different seeds (‘10’, ‘42’, ‘111’, ‘1111’, ‘1234’) while conducting experiments on the ILI-ENG data set for all test periods and forecasting horizons. The obtained results highlight that the proposed model provides consistent results across all regions and forecasting horizons. Results do not deviate significantly from the ones presented in the main paper (Table 1) which are obtained using seed ‘42’. Standard deviations in the averaged MAEs (all test periods) over the 5 seeds for each forecasting horizon do not exceed 0.07 which in real terms (using the units of the actual data) represents 7 people in a population of 10 million. This highlights the robustness of the mean estimate.

E.5 Analysis of model performance for tasks with strong seasonality

Prior work has shown that modelling inter-variable dependencies in time series problems may occasionally cause overfitting (Nie et al. 2023). While our results for the ILI and WEA forecasting tasks do not corroborate this (Section 4.2), we conduct further experiments on a different task (ELEC) that displays a different pattern of performance across most models. In these experiments, we explore different values for the parameter α in Sonnet. α controls the relative contribution of exogenous variables in the learned representations (section 3.1). For $\alpha = 0$, Sonnet only uses historical values of the target (endogenous) variable. We use the ELEC data set for evaluation because for this specific task, PatchTST—that does not capture inter-variable dependencies—outperforms some models that do (e.g. ModernTCN and Crossformer).

In addition, 7 out of 9 evaluated models cannot surpass the accuracy of the seasonal persistence model (both in terms of MAE and sMAPE), indicating that for ELEC, seasonal patterns are consistent over time. Sonnet’s hyperparameters are re-tuned (see Section 4.2 and Appendix D), except for α . Results for $\alpha = \{0, 0.25, 0.5, 0.75\}$ are enumerated in S12. The last row contains the performance of the seasonal persistence model (denoted as “Naïve”) with a seasonality set to 168 time steps (1 week).

We observe that although the prediction difference across different values of α is relatively small, Sonnet is consistently more accurate when setting $\alpha = 0$, i.e. when only historical values of the target variable are used and no exogenous variables are included. This indicates that for ELEC the exogenous inputs are not very informative. The performance of the seasonal persistence model also supports this conclusion given its strong performance for both years 2020 and 2021 ($r > 0.94$). This suggests that when strong seasonality is present, Sonnet benefits from following an autoregressive forecasting design without incorporating inter-variable dependencies (as α is a learnable parameter).

E.6 Computational cost of Sonnet

We analyse Sonnet’s computational cost w.r.t. 4 tunable hyperparameters: the number of atoms K , the size of the hidden dimension d , the length of the look-back window H , and the number of exogenous variables C . We analyse the influence of each variable independently by keeping the other three parameters fixed. Specifically, we set $d \in \{32, 64, 128, 256\}$ while having $K = 32$, $L = 112$, $C = 128$; similarly, we evaluate $K \in \{16, 32, 64, 128\}$, $L \in \{56, 84, 112, 224\}$, and $C \in \{64, 128, 256, 512\}$, while the other parameters are fixed to $d = 64$, $K = 32$, $L = 112$, and $C = 128$, respectively. The computational cost of each setup is obtained by averaging memory consumption over 100 epochs.

The GPU memory consumption of Sonnet during training is depicted in Figure S1. Sonnet’s GPU memory consumption stays constant as C increases. This is because the input is mapped to a fixed embedding space for modelling. For the other three parameters, the method shows a linear increase in GPU memory consumption.

E.7 Note on performance evaluation

We acknowledge that most prior work in time series forecasting evaluates model performance by averaging errors across

α	2020									2021								
	$H = 12$			$H = 24$			$H = 36$			$H = 12$			$H = 24$			$H = 36$		
	r	MAE	$\epsilon\%$															
0.75	0.9793	0.1085	25.62	0.9748	0.1214	27.44	0.9614	0.1514	33.14	0.9780	0.1073	24.87	0.9733	0.1192	26.85	0.9634	0.1457	30.39
0.5	0.9807	<u>0.1082</u>	25.73	0.9747	0.1247	28.25	0.9671	0.1456	31.41	0.9782	0.1108	25.82	<u>0.9747</u>	0.1185	26.82	0.9640	0.1421	30.88
0.25	0.9813	0.1093	25.93	0.9749	0.1250	29.17	0.9680	0.1430	31.69	0.9788	0.1111	26.03	0.9735	0.1209	26.65	0.9654	0.1434	30.56
0	0.9823	0.1036	25.30	0.9772	0.1179	26.96	0.9694	0.1401	31.25	0.9806	0.1042	24.56	0.9753	0.1170	27.09	0.9679	0.1308	28.91
Naïve	0.9461	0.1675	34.30	0.9461	0.1675	34.30	0.9461	0.1675	34.30	0.9412	0.1736	35.14	0.9412	0.1736	35.14	0.9412	0.1736	35.14

Table S12: Effect of different α values with Sonnet on the ELEC data set. r and $\epsilon\%$ denote the correlation and sMAPE scores, respectively. Best results are **bolded**, second best underlined.

Task	H	Sonnet	DeformTime	ModernTCN	Samformer	TimeXer	PatchTST	Itransformer	Crossformer	DLinear
ELEC	12	0.0885	<u>0.1033</u>	0.1440	0.1801	0.1114	0.1267	0.1261	0.1330	0.2630
	24	0.1034	<u>0.1223</u>	0.1649	0.2198	0.1423	0.1368	0.1394	0.1703	0.2997
	36	0.1138	0.1507	0.1788	0.2441	0.1546	<u>0.1431</u>	0.1554	0.1969	0.3259
ENER	24	<u>0.3152</u>	0.3474	0.3133	0.3256	0.3178	0.3262	0.3220	0.3205	0.3691
	48	0.3588	0.3962	<u>0.3692</u>	0.3715	0.4186	0.3791	0.3808	0.4253	0.4246
	72	0.3754	0.4071	<u>0.3792</u>	0.3814	0.4227	0.3867	0.3973	0.4123	0.4458
	168	0.3796	0.4620	<u>0.4175</u>	<u>0.3986</u>	0.4196	0.4352	0.3991	0.4772	0.4604
ETTh1	96	0.1972	0.1840	0.1774	0.1905	0.1807	0.1757	0.1825	0.1989	0.2045
	192	0.2187	0.1988	<u>0.2013</u>	0.2203	0.2043	0.1999	0.2051	0.2149	0.2834
	336	0.2462	0.2024	<u>0.2123</u>	0.2433	0.2226	0.2248	0.2322	0.2577	0.3877
	720	0.2661	0.2390	0.2288	0.2648	<u>0.2292</u>	0.2500	0.2449	0.3000	0.5007
ETTh2	96	0.2743	0.2924	0.2790	0.2986	0.2797	0.2765	0.2991	0.3254	0.2840
	192	0.3185	0.3010	0.3183	0.3254	0.3331	<u>0.3174</u>	0.3463	0.3534	0.3313
	336	0.3463	0.3172	<u>0.3350</u>	0.3622	0.3769	0.3417	0.3857	0.3891	0.4056
	720	<u>0.3729</u>	0.3577	<u>0.4259</u>	0.4239	0.4069	0.3887	0.3945	0.4248	0.5391
ILI-ENG	7	<u>1.3204</u>	1.2802	1.7351	1.7701	1.7086	1.9402	1.7746	1.3243	2.1892
	14	1.5964	<u>1.6521</u>	2.2656	2.1201	1.9703	2.4857	2.3660	1.9326	2.7452
	21	2.1226	<u>2.3246</u>	2.3331	2.8860	2.8852	2.8458	3.0904	2.8733	3.2983
	28	2.4956	2.7829	<u>2.5948</u>	3.3530	2.7894	3.2161	3.4784	3.0740	3.6805
ILI-US2	7	0.3795	<u>0.4142</u>	0.4523	0.5140	0.4931	0.6400	0.5455	0.4444	0.7214
	14	0.4186	<u>0.4544</u>	0.5501	0.5784	0.5402	0.7302	0.6357	0.4695	0.7899
	21	0.4914	<u>0.5374</u>	0.5576	0.6004	0.6190	0.7489	0.6554	0.5720	0.8642
	28	<u>0.5740</u>	0.5554	0.5892	0.6561	0.6808	0.8450	0.7370	0.5842	0.8920
ILI-US9	7	<u>0.2727</u>	0.2614	0.2945	0.3396	0.3435	0.3882	0.3725	0.3222	0.4348
	14	0.2925	0.3040	0.3398	0.3965	0.3715	0.4334	0.4049	0.3254	0.4780
	21	0.2955	<u>0.3187</u>	0.3558	0.3811	0.4430	0.4664	0.4504	0.3285	0.5315
	28	0.3671	0.3913	<u>0.3786</u>	0.4202	0.4774	0.5002	0.5535	0.4018	0.5622
WEA-CT	4	<u>1.1748</u>	1.3217	1.3716	1.6459	1.9038	2.8087	1.5908	1.1470	2.2270
	12	<u>2.4586</u>	2.5082	2.6260	2.9155	2.8796	3.6686	2.8671	2.3716	3.3320
	28	3.2135	3.3330	3.4816	3.4502	3.4469	3.6743	3.4602	3.2349	3.6682
	120	<u>3.6790</u>	3.7547	3.9605	3.8332	3.7892	3.9108	3.8934	3.6567	3.9094
WEA-HK	4	<u>0.5456</u>	0.6001	0.5729	0.6577	0.7984	0.9391	0.6449	0.5435	0.7752
	12	0.8753	0.9935	0.9314	0.9964	1.0159	1.2814	1.0259	0.8953	1.1804
	28	1.1809	1.2712	1.2761	1.3163	1.2920	1.3973	1.3405	<u>1.2660</u>	1.3926
	120	1.5093	1.6400	1.5321	1.6370	1.6032	1.7110	1.5684	<u>1.5196</u>	1.6268
WEA-LD	4	1.2448	1.4040	1.4175	1.5651	1.9055	2.2429	1.5485	1.2493	1.8231
	12	<u>2.2391</u>	2.3942	2.3661	2.4950	2.5732	2.9561	2.5287	2.2368	2.7131
	28	2.8627	3.0055	2.9744	3.0418	3.0354	3.2615	3.1209	2.8913	3.1500
	120	3.2539	<u>3.3166</u>	3.6610	3.5329	3.5188	3.7507	3.6614	3.3583	3.6064
WEA-NY	4	0.9584	1.1266	1.0886	1.2500	1.5107	1.7682	1.2372	<u>0.9673</u>	1.4818
	12	1.7458	1.8459	1.8486	1.9756	2.1140	2.3498	1.9589	<u>1.7531</u>	2.2809
	28	2.2952	2.4040	2.4314	2.5138	2.5193	2.6537	2.5108	<u>2.3223</u>	2.7166
	120	2.6635	2.8076	2.9735	2.9731	2.9984	2.9692	2.7759	<u>2.7372</u>	3.1808
WEA-SG	4	0.3109	0.3229	0.3243	0.3622	0.3596	0.4010	0.3542	<u>0.3132</u>	0.3809
	12	0.3664	0.3849	0.3899	0.4189	0.4020	0.4487	0.4099	<u>0.3765</u>	0.4285
	28	0.4213	0.4540	0.4565	0.4713	0.4475	0.4866	0.4655	<u>0.4414</u>	0.4719
	120	0.4747	0.5128	0.5101	0.5018	0.5023	0.5191	<u>0.4936</u>	0.4980	0.5151

Table S13: Mean Absolute Error (MAE) evaluated over the full predicted sequence for all forecasting horizons (H), tasks, and models. In consistency with the main experimental setup, error metrics are averaged over 4 test seasons for ILI tasks, 3 years for the WEA tasks, and 2 for ELEC. Best results are **bolded**, second best underlined.

the entire prediction horizon. While this provides a general view of forecasting accuracy, it may obscure performance at the target time step. As the prediction horizon extends, forecasting becomes more challenging (Hyndman and Koehler 2006). Model performance can thus vary significantly between forecasting the closer / further time steps. For example, consider two models whose predictions over a three-step sequence yield MAEs of $\{0.1, 0.2, 0.6\}$ and $\{0.2, 0.3, 0.4\}$, respectively. While both models have the same averaged MAE when evaluated over the sequence, the second model

performs better on the final time step, which is the main forecasting target. Averaging errors over all time steps may benefit models that excel in early predictions but struggle near the target horizon. We further demonstrate this point in the coming section with empirical results.

E.8 Evaluating forecasts over the entire output sequence

To provide a more comprehensive understanding of model performance, we also provide the forecasting accuracy by

averaging the error across the entire output sequence, as opposed to just using the target time step (Table 1). The results are presented in Table S13. It can be observed that Sonnet ranks first in 31 over 47 tasks and second in 9 tasks. The averaged MAE reduction is 1.0%. Additionally, Sonnet reduces the MAE of DeformTime, which is the best-performing baseline, by 4.7%.

For the ILI and WEA data sets, the best-performing baseline is DeformTime when evaluated at the target time step, with Sonnet reducing the MAE by 3.3% on average. However, Crossformer is the best performing model when evaluated over the sequence, with Sonnet reducing the MAE by 5.4%. This observation indicates that DeformTime performs better than Crossformer at the target horizon, while Crossformer yields better performance when considering the entire series of forecasts. This change in the ranking of baselines supports our argument in Section E.7 that averaging errors across the sequence, rather than evaluating the error at the target forecasting horizon, can lead to a misleading assessment of how the model performs at different forecasting horizons.

F Limitations

The main limitation is that the validity and predictiveness of the proposed method are only verified empirically (through experiments) but not theoretically. To mitigate against this, we have conducted extensive experiments over a wide range of data sets and tasks, covering different application fields. Many (8) of the data sets involve multiple test seasons (hence, multiple training / testing trials can be conducted), and have training sets that encompass time spans longer than a decade. Nevertheless, we acknowledge that additional evaluation across a broader range of forecasting problems could have provided an even more comprehensive assessment.

As far as the MVCA module is concerned (a key contribution of Sonnet), we argue that it is a direct and effective replacement for naïve attention in time series forecasting models. Although our current experiments support this claim, we nevertheless acknowledge that further analysis is needed to better understand its impact across a wider range of applications. Such insights could help guide more informed replacements of attention mechanisms in future work.

Finally, Sonnet—and many other SOTA forecasting models—cannot be considered as an interpretable model. We cannot know why Sonnet makes a certain forecast and we cannot directly attribute this to specific parts of the endogenous input. This can only be approximated through meta-analysis.

G Supplementary ILI rate forecasting figures

In this section, a series of figures is shown below for the ILI rate prediction task, where each figure corresponds to a particular forecasting window and location, showcasing outputs from all models in parallel for comparison.

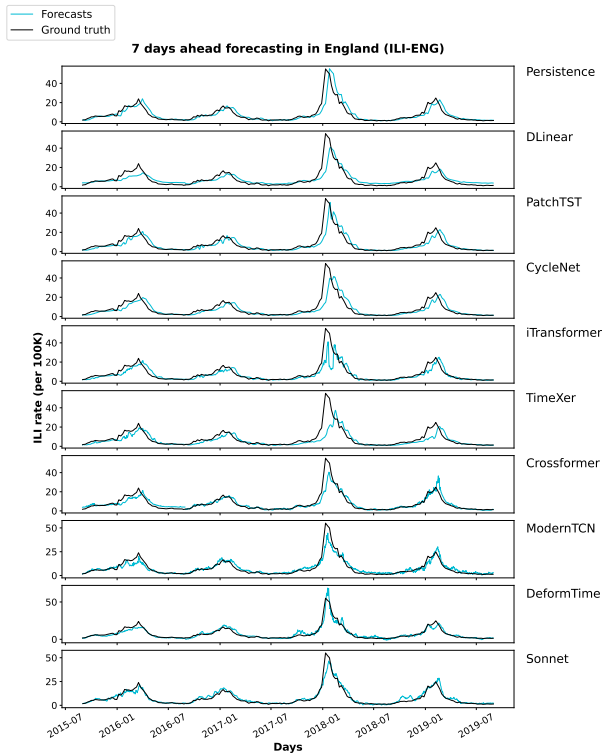


Figure S2: 7-day ahead forecasts for all influenza seasons and models, England (ILI-ENG).

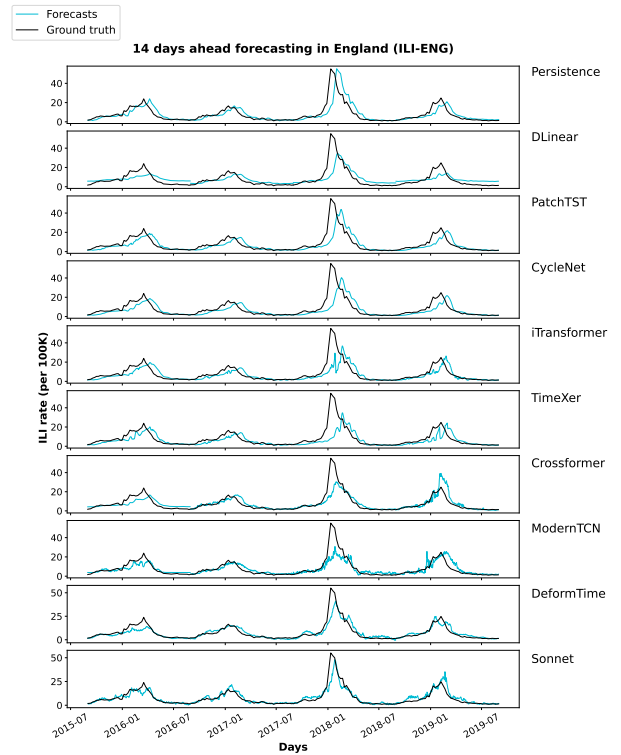


Figure S3: 14-day ahead forecasts for all influenza seasons and models, England (ILI-ENG).

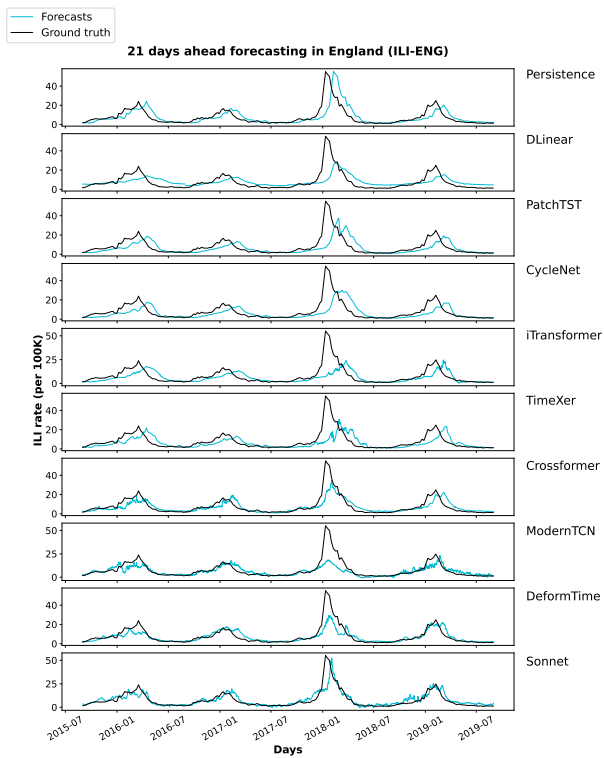


Figure S4: 21-day ahead forecasts for all influenza seasons and models, England (ILI-ENG).

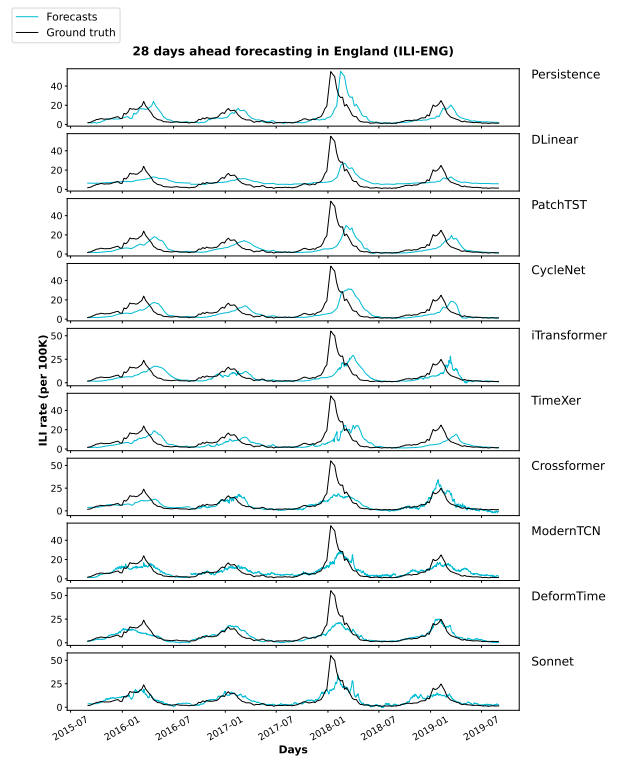


Figure S5: 28-day ahead forecasts for all influenza seasons and models, England (ILI-ENG).

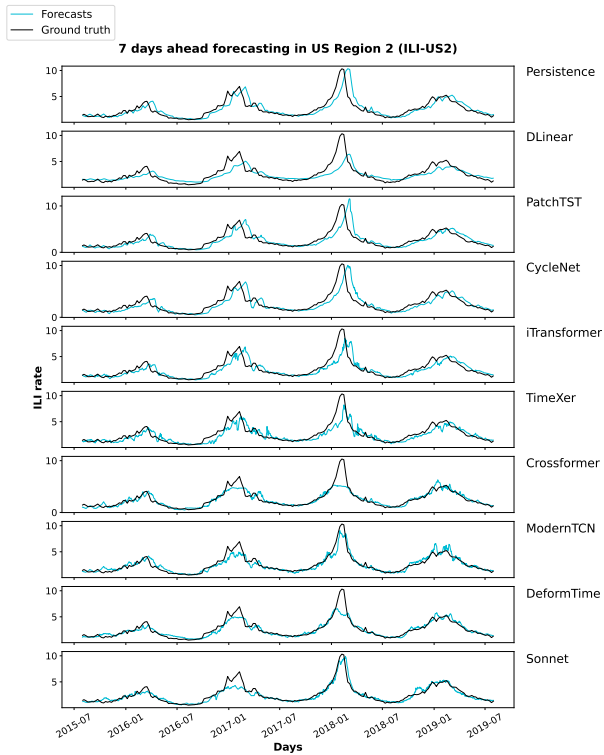


Figure S6: 7-day ahead forecasts for all influenza seasons and models, US Region 2 (ILI-US2).

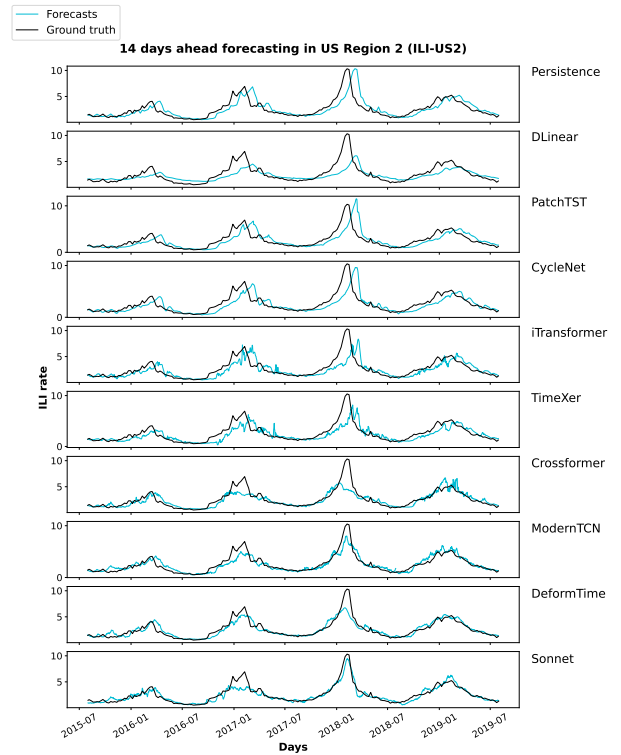


Figure S7: 14-day ahead forecasts for all influenza seasons and models, US Region 2 (ILI-US2).

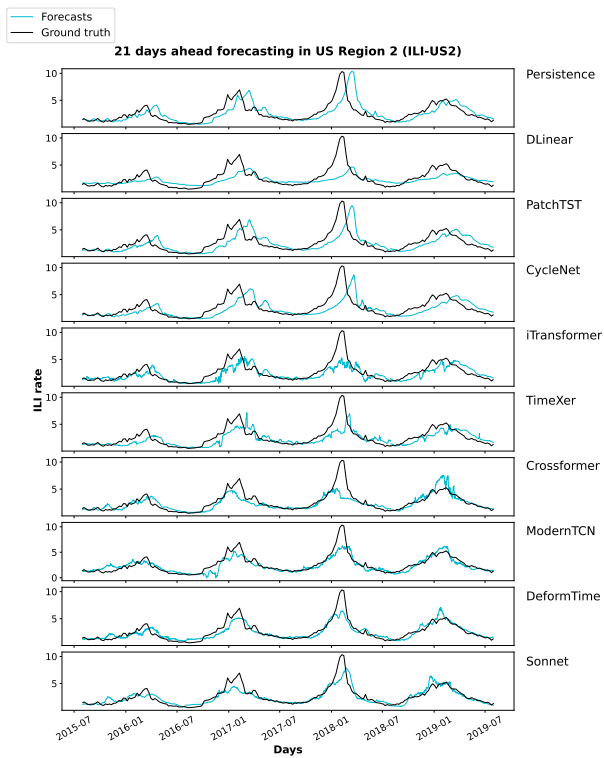


Figure S8: 21-day ahead forecasts for all influenza seasons and models, US Region 2 (ILI-US2).

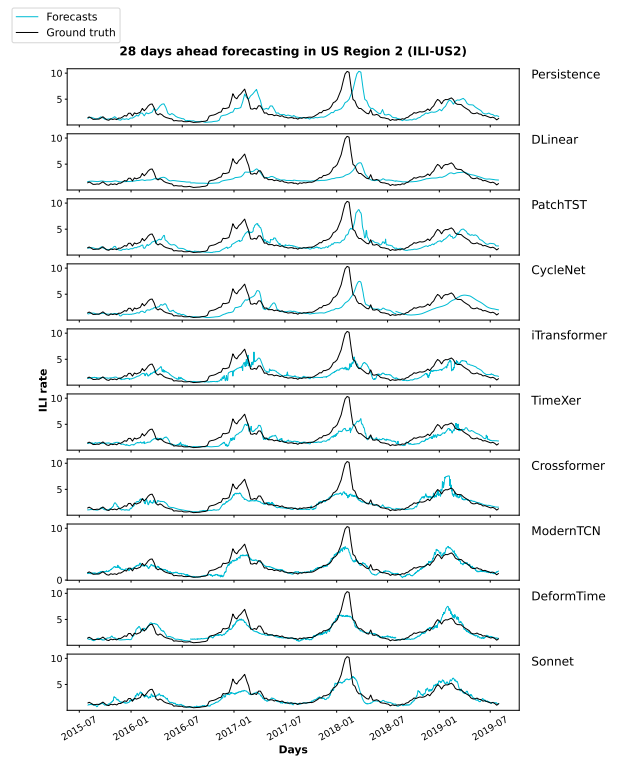


Figure S9: 28-day ahead forecasts for all influenza seasons and models, US Region 2 (ILI-US2).

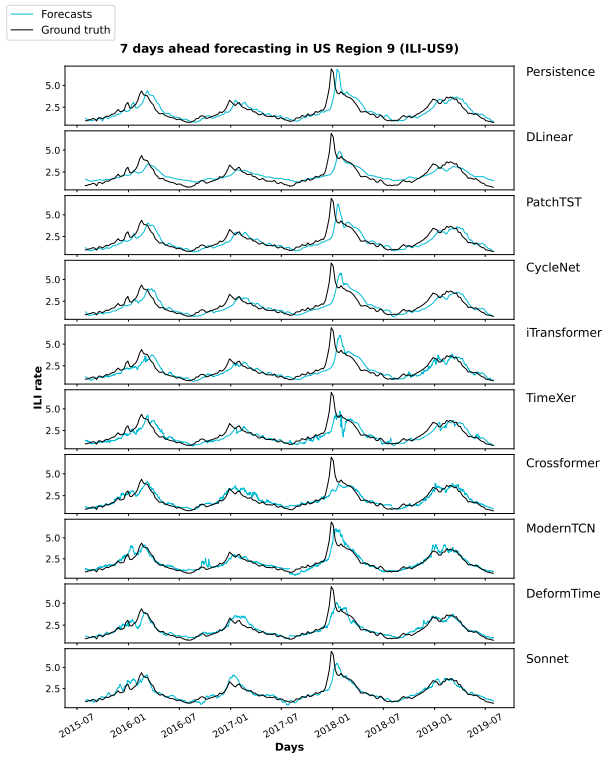


Figure S10: 7-day ahead forecasts for all influenza seasons and models, US Region 9 (ILI-US9).

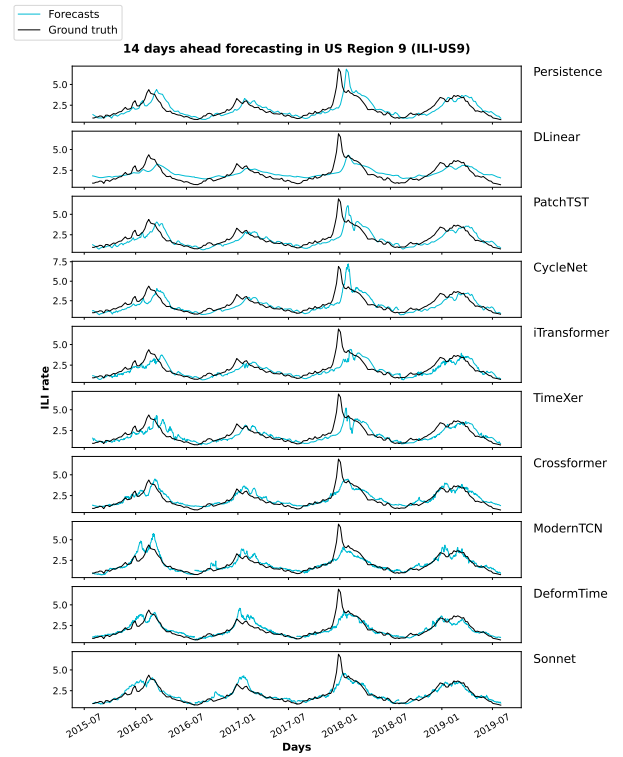


Figure S11: 14-day ahead forecasts for all influenza seasons and models, US Region 9 (ILI-US9).

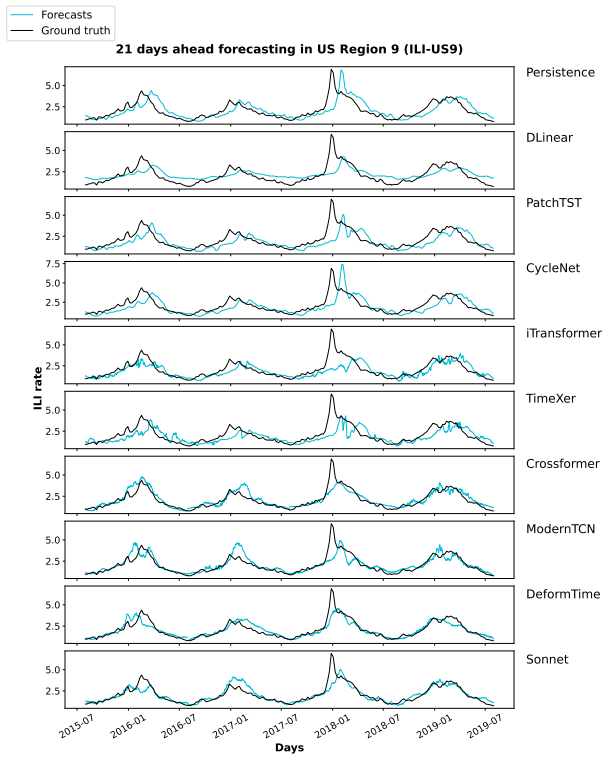


Figure S12: 21-day ahead forecasts for all influenza seasons and models, US Region 9 (ILI-US9).

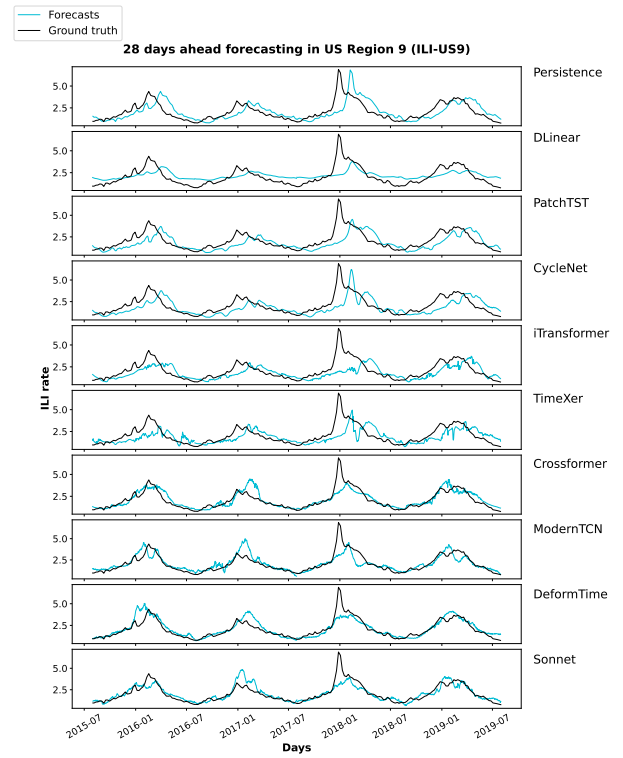


Figure S13: 28-day ahead forecasts for all influenza seasons and models, US Region 9 (ILI-US9).